Ore Geology Reviews 127 (2020) 103840

Contents lists available at ScienceDirect

Ore Geology Reviews

journal homepage: www.elsevier.com/locate/oregeorev

Geochemical and mineralogical diagnosis on gold ores: A case study from the Cadillac–Larder Lake Fault Zone, Abitibi, Canada

Yu-Miao Meng [a,b,*], Michel Jébrak [b], Christian Sasseville [b,c], Xiao-Wen Huang [a]

[a] State Key Laboratory of Ore Deposit Geochemistry, Institute of Geochemistry, Chinese Academy of Sciences, Guiyang 550081, China
[b] Département des Sciences de la Terre et de l'Atmosphère, Université du Québec à Montréal (UQÀM), Montréal, QC H3C 3P8, Canada
[c] Coopérative de Solidarité GÉOCOOP, Montréal, QC H1K 5G6, Canada

ARTICLE INFO

Keywords:
Gold deposit
Principal component analysis
Geochemistry
Mineralogy
Mineral exploration
Abitibi

ABSTRACT

Numerous orogenic gold deposits have been discovered within the Archean Abitibi greenstone belt of Canada. These include the Francoeur, Wasamac, Astoria, Zulapa, Goldex, Lamaque, Lac Herbin, and Beaufor deposits, all of which are located within the Cadillac–Larder Lake Fault Zone (CLLFZ). These gold deposits are hosted by various lithologies and vary in terms of style of mineralization, sulfide abundance, and hydrothermal alteration. These variations mean that exploration for new deposits has been difficult in this area using common exploration criteria. This study presents the results of a principal component analysis (PCA)-based approach, combining geochemical and mineralogical data to quickly identify different types of gold mineralization within the CLLFZ, including assessing the use of this approach in mineral exploration.

The first principal components in both classification methods used during this study (PC_E1 and PC_M1, representing element geochemical and mineralogical classification respectively) can efficiently discriminate between mineralization and barren/altered rocks. The second principal components (PC_E2 and PC_M2) can be used to constrain the host rocks (altered vs. barren) and style of mineralization (disseminated vs. vein-hosted), respectively. Finally, PC_E3 and PC_M3 give more detailed information on the nature of the mineralization in an area, possible reflecting variations in the composition of ore-forming fluids. All of the above indicates that the two PC_E and PC_M classification methods are complementary, which means that using approaches that combine these methods will provide a comprehensive understanding of the nature of studied samples and/or deposits.

Information extracted from the results of the PCA undertaken during this study may be beneficial for mineral exploration in unknown districts, such as glaciated areas, where traditional geological fieldwork is challenging. This study also defines element and mineral mineralization indices based on PC_E1 and PC_M1, which enables evaluation of the extent and style of gold mineralization in an area. This study indicates that PCA-based automated mineralogical and geochemical classification methods could be highly useful in exploration for gold deposits.

1. Introduction

Orogenic lode gold deposits generally form within compressional to transpressional crustal-scale fault zones in Archean greenstone belts (Colvine et al., 1984; Rabeau et al., 2013; Groves et al., 2018). These major structures act as important channels for hydrothermal fluids (Beaudoin and Pitre, 2005; Goldfarb et al., 2005). Numerous orogenic lode gold deposits are located along the Destor–Porcupine Fault Zone and the Cadillac–Larder Lake Fault Zone (CLLFZ) within the Archean Abitibi greenstone belt of the Superior Craton, Canada (Fig. 1). The CLLFZ accounts for half of the gold production and reserves in the Abitibi Province, and >25% of the gold production and reserves in Canada (Dubé et al., 2007). The zone has produced >4200 t Au, and contains 37 world-class (>10 t Au) gold deposits and 4 giant gold districts (>100 t Au). As such, the CLLFZ represents one of the most important gold metallogenic districts in the world (Dubé et al., 2007).

Orogenic gold deposits are associated with characteristic types and styles of alteration and mineralization (Goldfarb et al., 2001; Trépanier et al., 2015) and detailed analysis of alteration zoning can provide vectors for gold mineralization (Eilu and Mikucki, 1998; Crosta et al., 2003; Gaillard et al., 2018). Specific mineral assemblages in alteration zones can also provide information on the prevailing temperature,

* Corresponding author at: State Key Laboratory of Ore Deposit Geochemistry, Institute of Geochemistry, Chinese Academy of Sciences, Guiyang 550081, China.
E-mail address: mengyumiao@mail.gyig.ac.cn (Y.-M. Meng).

https://doi.org/10.1016/j.oregeorev.2020.103840
Received 23 June 2020; Received in revised form 7 October 2020; Accepted 12 October 2020
Available online 15 October 2020

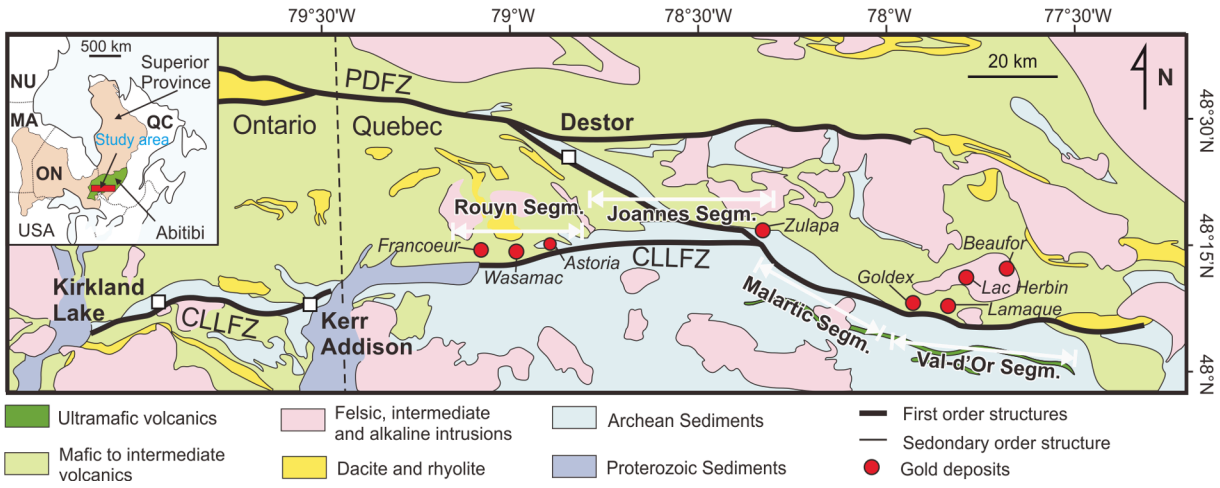

Fig. 1. Map showing the main structural corridors of southern Abitibi, namely the Cadillac–Larder Lake Fault Zone (CLLFZ) and the Destor–Porcupine Fault Zone (PDFZ; modified from Robert, 2001, Rabeau et al., 2013, and Rafini, 2014). The location of the gold deposits that form the focus of this study are also shown. Structural segment divisions are after Bedeaux et al. (2017).

Table 1
Characteristics of the different gold mineralization styles spatially associated to the CLLFZ in Abitibi of Canada.

Deposit	Francoeur	Wasamac	Astoria	Zulapa	Goldex	Lamaque	Lac Herbin	Beaufor
Segment	Rouyn	Rouyn	Rouyn	Joannes	Val-d'Or	Val-d'Or	Val-d'Or	Val-d'Or
Tonnages and grades	0.6 Mt @ 6.91 g/t Au (Probable)	21.45 Mt @ 2.56 g/t (Proven + Probable)	2.9 Mt @ 4 g/t Au (Proven + Probable)	1.12 Mt @ 7.24 g/t Au (Proven); 1.71 Mt @ 7.56 g/t Au (Probable)	14.8 Mt @ 1.87 g/t Au (Proven); 13.0 Mt @ 1.62 g/t Au (Probable)	24 Mt @ 5.9 g/t Au (Proven + Probable)	43,000 t @ 7.45 g/t Au (Proven); 96,000 t @ 6.45 g/t Au (Probable)	81,742 t @ 7.53 g/t Au (Proven); 201,296 t @ 7.6 g/t Au (Probable)
Mineralization style	Disseminated pyrite	Disseminated pyrite	Tabular, stockwork	Sulfide-rich veins	Tourmaline veins	Tourmaline veins	Tourmaline veins	Tourmaline veins
Sulfide abundance	Medium to high (7–40%)	Medium to high (7–40%)	Low (<5%)	Medium (10–15%)	High (up to 25%)	High (up to 25%)	High (up to 25%)	High (up to 25%)
Sulfide nature	Pyrite	Pyrite	Pyrite, arsenopyrite, gersdorffite, chalcopyrite	Pyrite, arsenopyrite, pyrrhotite	Pyrite	Pyrite, chalcopyrite, pyrrhotite, tellurium	Pyrite, pyrrhotite, chalcopyrite, sphalerite, galena, cobaltite, tellurides	Pyrite and chalcopyrite
Alteration	Carbonate, hematite, muscovite, albite	Microcline, carbonates quartz, albite, sericite	Carbonate, fuchsite, sericite	Biotite	Albite, sericite, biotite, chlorite	Carbonate, sericite, pyrite, minor albite	Carbonate, white mica, chlorite	chlorite, sericite, carbonate
Host rock	Mafic to felsic metavolcanic schists and abitite dykes	Mafic to felsic metavolcanic schists and abitite dykes	Mafic and ultramafic metavolcanites and clastic sediments	Mafic to ultramafic rocks	Tonalitic to dioritic intrusion	Diorite intrusions	Diorite	Granodiorite

Note: This table is compiled according to Rafini (2014) and Bedeaux et al. (2017). Tonnages and grades data: Lamaque-Cowan (2020), Wasamac-NS Energy Company, Astoria- Yorbeau Resources Inc., data for Francoeur, Zulapa, Goldex, Lac Herbin and Beaufor are from Natural Resources Canada (https://www.nrcan.gc.ca/mining-materials/exploration/8294).

pressure, and fluid composition during mineralization, providing important constraints on ore deposit models (Colvine et al., 1984; Groves et al., 1998; McCuaig and Kerrich, 1998; Goldfarb et al., 2005). However, the intensity, range, and mineral assemblages formed during alteration vary with changes in host rock lithology and crustal depth (Colvine, 1989; Groves et al., 1998; Goldfarb et al., 2005). In addition, poor exposure levels in glaciated areas mean that alteration features can be difficult to identify. This means that identifying the type of mineralization in new areas on the basis of alteration is challenging during the early stages of mineral exploration. In addition to the variations in alteration discussed above, orogenic gold deposits also contain different types of mineralization that reflect the influences of different faulting regimes (Robert et al., 1995, 2005; Robert and Poulsen, 2001; Sibson, 2004; Rafini, 2014). Ore deposit formation under brittle faulting conditions is typically associated with mineralized stockworks and breccias, whereas ductile conditions are typically associated with disseminated mineralization that is hosted by deformed stratiform veins (Goldfarb et al., 2005). Mineralization within the brittle–ductile transition zone is generally hosted by discordant or concordant quartz–carbonate or S-type veins (Goldfarb et al., 2005). This adds a level of complexity to mineral exploration, as the presence of disseminated mineralization in an area can often be overlooked if detailed mineralogical and geochemical analyses are not undertaken.

Previous research has outlined the geochronology, tectonic evolution, and ore-forming processes involved in the formation of Archean greenstone-hosted orogenic gold deposits within the Abitibi Province (Robert, 1990; Wong et al., 1991; Beaudoin and Pitre, 2005; Goldfarb et al., 2005; Neumayr et al., 2007; Rabeau et al., 2013; McNicoll et al.,

2014; Rafini, 2014; Beaudoin and Chiaradia, 2016; Fayol et al., 2016; De Souza et al., 2017; Dubé et al., 2017; Mercier-Langevin et al., 2017; Poulsen et al., 2017; Rezeau et al., 2017). Some of these studies determined that individual deposits can contain different types of mineralization and alteration (Robert and Poulsen, 1997; Neumayr et al., 2000; Beaudoin and Pitre, 2005; Rabeau et al., 2013). Gold deposits within the CLLFZ exhibit different types of mineralization, have different geometries, sulfide abundances, and host rocks, and are associated with hydrothermal alteration (Table 1; Rafini, 2014; Bedeaux et al., 2017; De Souza et al., 2017; Dubé et al., 2017; Mercier-Langevin et al., 2017). The mineralization within this area includes tabular stockwork, disseminated pyrite, sulfide-rich vein, stockwork–disseminated, albite vein, and tourmaline vein mineralization types (Table 1; Rafini, 2014; Bedeaux et al., 2017). The mineralization is associated with various types of carbonate alteration, silicification, and alkali metasomatism (e.g., potassic and sodic alteration). Variations in alteration and mineralization types within individual deposits in this region makes mineral exploration challenging, because not all exploration criteria are applicable to all of the deposits in this area, or even to different parts of the same deposit. This makes it impossible to establish clear quantitative relationships between gold grades and the given features of a deposit. As such, a rapid, quantitative method is needed for characterizing deposits based on limited surface exposure, or from samples from drill cores only.

This paper outlines the chemical composition and mineralogy of mineralized samples from eight orogenic gold deposits within the Abitibi Province. These deposits include the Francoeur, Wasamac, Astoria, Zulapa, Goldex, Lamaque, Lac Herbin, and Beaufor deposits, from west to east along the CLLFZ (Fig. 1). This multidimensional dataset contains abundant information about the alteration and mineralization characteristics of these eight deposits. Commonly used binary plots or multi-element variation diagrams appear to capture only specific information on mineralization and alteration within these deposits. However, principal component analysis (PCA), which is an effective data dimension reduction method based on covariations between variables, can reveal information that is otherwise hidden within individual datasets (Grunsky, 2010). This approach has been widely used for provenance discrimination and mineral exploration (e.g., Chandrajith et al., 2001; Cheng et al., 2011; Makvandi et al., 2016; Chen et al., 2018). This study uses PCA to extract important information about alteration and mineralization that can be used to discriminate between different types of gold deposit. This approach demonstrates that geochemical and mineralogical classification can provide diagnostic information about variations in host rock lithologies, mineralization and alteration types, and the formation of mineralized veins. Both of the methods outlined in this study can efficiently discriminate between mineralized and barren/altered rocks; however, the mineralogical classification method discriminates between different styles of mineralization, whereas the geochemical classification method discriminates between altered and unaltered rocks. This means that the classification methods are complementary, with a combined approach being potentially useful during exploration for gold deposits within poorly studied or poorly exposed districts.

2. Geological background

The Abitibi metallogenic province within the southwestern Superior Province is the largest greenstone belt in the Canadian Shield and covers an area of 700 × 300 km (Fig. 1). The southern Abitibi greenstone belt contains metavolcanic units of the Blake River, Malartic, and Louvicourt groups and the Piché structural complex, all which are ultramafic to felsic in composition and are tholeiitic to calc-alkaline (Goodwin, 1982; Corfu, 1993; Scott et al., 2002; McNicoll et al., 2014; Monecke et al., 2017). Archean sedimentary units that overlie these metavolcanic units include the flysch-type Cadillac and Kewagama groups, the turbiditic Pontiac Group, and the Timiskaming Group, which contains polymict conglomerates, sandstones, and argillites (Bedeaux et al., 2017). The belt has undergone regional sub-greenschist to greenschist–amphibolite transitional facies metamorphism, with deeper parts of the crust exposed with increasing proximity to the Proterozoic Grenville Front (Powell et al., 1995). The metamorphism within the southern Abitibi greenstone belt occurred between ca. 2680 and ca. 2640 Ma (Jolly, 1978; Powell et al., 1995; Dubé et al., 2007).

The CLLFZ is an east–west trending crustal discontinuity that extends for around 250 km (Bedeaux et al., 2017), and separates the Abitibi and Pontiac sub-provinces in Quebec (Fig. 1). The structural evolution of the CLLFZ is divided into four major events, the two most important of which are a late Archean N–S shortening event and a later NW–SE shortening event that was coincident with dextral strike-slip movements (Wilkinson et al., 1999; Daigneault et al., 2002, 2004; Bedeaux et al., 2017). Numerous gold deposits with diverse styles of mineralization and alteration cluster in regional-scale goldfields along the CLLFZ (Couture et al., 1994; Robert and Poulsen, 1997; Neumayr et al., 2000; Beaudoin and Pitre, 2005; Rabeau et al., 2013; Rafini, 2014). The CLLFZ can be subdivided into four segments according to changes in deformation patterns, namely (from west to east) the moderately north-plunging Rouyn, subvertical to west-plunging Joannes, steeply NE-plunging Malartic, and steeply north-plunging Val-d'Or segments (Bedeaux et al., 2017). Structural heterogeneities within the CLLFZ led to persistent seismic segmentation and repeated rupturing of the same fault windows (Bedeaux et al., 2017). These ruptures enhanced the permeability of large-scale fluid migration channels, thereby acting as a control on the hydrothermal activity within the southern Abitibi greenstone belt and the resulting distribution of gold deposits (Bedeaux et al., 2017, 2018).

2.1. Rouyn segment

The Rouyn segment of the CLLFZ is the westernmost part of the zone and extends 50 km from west to east (Fig. 1). This segment contains stockwork–veinlet and disseminated sulfide mineralization that is hosted by ultramafic and mafic rocks and albitite dikes (Bedeaux et al., 2017; Mériaud and Jébrak, 2017). The veins have low sulfide abundances (<5%), whereas the stockwork–veinlet and disseminated styles of mineralization contain 7%–40% sulfides. The sulfides are dominated by pyrite, arsenopyrite, and chalcopyrite, and are associated with carbonate, fuchsite, and albite alteration.

The Francoeur and Wasamac gold deposits within the Rouyn segment were selected as representative examples of the disseminated pyrite style of gold mineralization. Both deposits are located along a second-order reverse structure related to the CLLFZ (Couture and Pilote, 1993), and have pyrite-dominated sulfide assemblages that are disseminated within mylonitic foliations. The mineralization is hosted by mafic to felsic metavolcanic schists of the Blake River Group and albitite dikes. The deposits are associated with: (1) Early pervasive, pre-ore, low-temperature K–Fe hydrothermal alteration that forms carbonates, hematite, and muscovite; (2) a gold mineralization-related albite–pyrite phase of alteration; and (3) post-ore alteration associated with the formation of gypsum and anhydrite veinlets (Couture and Pilote, 1993). The Wasamac gold deposit is also associated with potassic (microcline, carbonate, and quartz) and sodic (albite, sericite, and carbonate) alteration that occur together (Mériaud and Jébrak, 2017). The Astoria gold deposit is classified as a quartz vein-dominated tabular stockwork deposit, and was studied for comparative purposes. It is hosted by mafic and ultramafic metavolcanic rocks of the Piché structural complex and clastic sediments of the Timiskaming Group, both of which have undergone intense carbonate–fuchsite (+sericite) alteration (Rafini, 2014). The sulfide assemblage within the deposit is dominated by arsenopyrite, gersdorffite, pyrite, and chalcopyrite associated with free native gold (Table 1).

2.2. Joannes segment

The Joannes segment is 40 km long, strikes east–west, and is

geometrically separated from the Malartic segment to the east. This segment contains semi-massive vein- and veinlet-type gold mineralization that contains 10%–15% sulfides. These sulfides are dominated by pyrite with arsenopyrite and pyrrhotite, and are associated with biotite alteration (Rafini, 2014; Bedeaux et al., 2017). The mineralization is hosted in a *syn*-tectonic intrusion and surrounding banded iron formation units.

The Zulapa gold deposit was chosen as a representative example of the sulfide-rich vein-hosted mineralization in this segment. The gold mineralization within the deposit is hosted predominantly by mafic to ultramafic rocks of the Piché Group that have been significantly deformed, metamorphosed (under upper greenschist–lower amphibolite facies conditions), and altered (Simard et al., 2013). Gold mineralization is present as invisible gold within arsenopyrite + pyrrhotite ± pyrite sulfide assemblages, as native gold disseminated within hydrothermally altered wall rocks (Simard et al., 2013), and locally in quartz–carbonate veinlets. The precipitation of auriferous arsenopyrite may be related to potassic alteration, as evidenced by the close spatial association between biotite-altered wall rocks and arsenopyrite (Simard et al., 2013).

2.3. Val-d'Or segment

The Val-d'Or segment is 70 km long and located in the eastern CLLFZ (Fig. 1). The Bourlamaque quartz diorite pluton hosts a number of gold deposits (Jébrak et al., 1991), and has an ovoid shape with a long axis parallel to the dominant regional E–W-trending structure in this area (Jébrak et al., 1991). This pluton is thought to have formed during the same volcanic and magmatic event that formed the Val-d'Or Formation (Belkabir et al., 1993; Kerrich and King, 1993; Faure, 2009).

Two types of gold deposit have been identified within the Val-d'Or sediment, namely (1) disseminated gold with sulfides, hosted by massive, fractured, or brecciated wall rocks, and (2) vein-type deposits (Robert, 1990, 1994; Jébrak et al., 1991; Couture et al., 1994). The majority of the gold within this segment is hosted by massive quartz–carbonate–tourmaline–chlorite–scheelite veins (Bedeaux et al., 2017) that contain up to 25% sulfides, with an assemblage dominated by pyrite and chalcopyrite. The alteration within this segment is dominated by chlorite, sericite, and carbonate alteration (Bedeaux et al., 2017).

The Goldex, Lamaque, Lac Herbin, and Beaufor deposits within the Val-d'Or segment were selected for analysis in this study. The Goldex gold mine is located 4 km west of the town of Val-d'Or. The mineralization within the deposit is hosted by gold-bearing quartz–tourmaline veins that are located within a quartz diorite and granodiorite sill (Hudyma et al., 2010; Daver et al., 2015; Daver, 2017). The gold within the deposit is hosted predominantly by pyrite, and is associated with sericite, albite, and chlorite alteration (Bedeaux et al., 2017).

The Lamaque gold deposit is located to the south of the Bourlamaque pluton and is hosted in a diorite that intersects the Val-d'Or Formation. It is connected to a third-order fault system associated with the CLLFZ (Neumayr et al., 2000, 2007) and has produced >140 t of Au, with some mineralized zones within the deposit remaining unexploited (Poirier et al., 2005). These include the Triangle and Parallel zones that are separated by 2 km, with the former lying to the southeast of the latter (Poirier et al., 2005). The deposit is dominated by a pyrite, chalcopyrite, pyrrhotite, and tellurium mineralized assemblage that is associated with carbonate, sericite, pyrite and albite alteration. The mineralization is also associated with quartz, tourmaline, calcite, chlorite, scheelite, and albite (Sasseville et al., 2015; Kreuzer et al., 2019).

The Lac Herbin gold deposit is hosted by the Bourlamaque granodiorite pluton (Lemarchand, 2012), and consists of a number of subvertical and subhorizontal quartz–tourmaline–carbonate fault-fill veins (Rezeau et al., 2017). This mineralization is associated with carbonate, white mica, chlorite, and albite alteration (Rezeau et al., 2017). The mineralization contains abundant, locally semi-massive pyrite and pyrrhotite, with minor amounts of chalcopyrite. Gold is predominantly hosted by fractures within deformed pyrite and quartz associated with chalcopyrite and carbonate (Lemarchand, 2012; Rezeau et al., 2017).

The Beaufor gold mine is located in Val-d'Or, to the east of the Bourlamaque pluton. This deposit hosts several auriferous quartz–tourmaline–carbonate veins (Tremblay, 2001) that contain sulfide assemblages dominated by pyrite and chalcopyrite. The gold in the deposit is closely associated with pyrite. The alteration in this area is characterized by a bleached inner zone associated with chlorite, sericite, and carbonate alteration, which gives way to an outer zone containing hydrothermal chlorite and igneous plagioclase (Tessier et al., 1990).

3. Methodology

3.1. Sample and method selection

The samples used during this study were either mineralized or altered samples from the eight southern Abitibi deposits outlined above. These deposits are located in different structural segments (Fig. 1) and are associated with different host lithologies, sulfide abundances, alteration, and types of mineralization (Table 1). The selected deposits are representative examples of the main mineralization types in the Abitibi area. The approach used during this study involved the selection of single samples for each deposit, the majority of which were divided into subsamples based on a size-fraction approach. Sample selection relied on discussions with mine operators to ensure the samples used were representative of the mineralization within each deposit. Samples that contained veins were prepared to include both vein and wall rock materials. Pyrite separates from the same samples (i.e., subsamples) have been used previously for Re–Os isotope dating of these deposits (Sasseville and Jébrak, 2017), as well as trace element analysis (Daver et al., 2020). Tourmaline separates from the same sample set have also been used for B isotope and trace element analyses (Daver et al., 2020). This meant that a systematic dataset that included data obtained previously from the same samples and size fractions were available for use during this study, which allows the linkage of features within the deposits, such as alteration and mineralization, with variations in the timing of formation and fluid evolution within these mineralizing systems. The size-fraction sampling approach used was originally designed for the separation of pyrite for Re–Os isotope analysis, and this approach can potentially discriminate between different generations of pyrite or sulfides that contain different concentrations of Re and Au. In addition, the more data used in a multivariate statistical analysis with fixed variables, the more the reliable results. The size-fraction method divides one sample into a few subsamples, increasing the amount of available data and furthering the ability to determine any potential impact of particle size distribution on the resulting data.

3.2. Size-fraction approach to sample separation

The methodology used here was based on that outlined by Clauer and Chaudhuri (1998) and built on by Sasseville et al. (2015) and Meng et al. (2017). In this study, the size-fraction approach entailed the use of samples that are first crushed by a manual cast-steel jaw crusher before disaggregation by grinding for 1–2 min in an electric rotary agate mortar. The resulting ground samples were then sorted into different size fractions by sieving with an aliquot of material reserved for use as a whole-rock sample. The remaining samples were sieved with USA standard test sieves, which yielded eight size fractions at >1000, 500–1000, 250–500, 100–250, 60–100, 40–60, and <40 μm. An aliquot of each fraction was kept dry for use in X-ray fluorescence (XRF) and X-ray diffraction (XRD) analyses, ensuring that soluble minerals such as anhydrite and various salts were not lost as a result of their solubility. Traditional chemical dissolution methods, such as those used for inductively coupled plasma–mass spectrometry (ICP–MS or ICP–atomic emission spectrometry (AES), require time consuming, expensive, and hazardous sample preparation techniques. In comparison, XRF and XRD analyses yield non-destructive, fast, and low-cost geochemical and

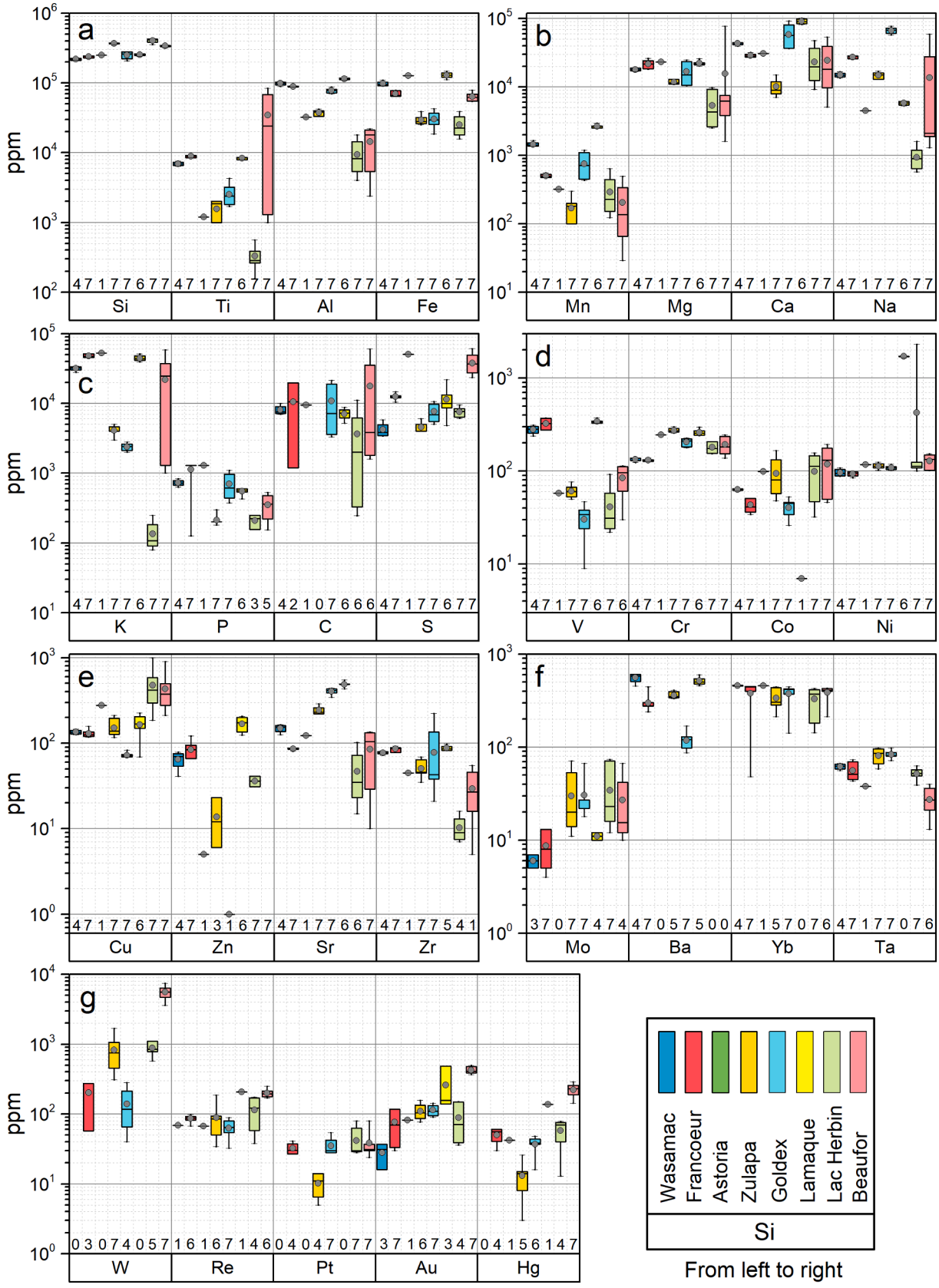

Fig. 2. Box and whisker plots showing variations in major and trace element concentrations within mineralized rocks from orogenic gold deposits of the Abitibi. Whiskers represent the range of minimum and maximum values, and the short line within each box represents the median value, which separates the box into two parts (i.e., lower 25–50 and upper 50–75 percentile groups). The gray filled circle represents the average value, and the number along the x-axis indicates the number of analyses undertaken for each deposit.

mineralogical information, respectively.

3.3. XRF analysis

A total of 46 size-distribution fractions and whole-rock samples were analyzed using a Bruker S-4 Pioneer XRF instrument at the University of Quebec at Montreal, Montreal, Quebec, Canada (UQÀM). This analysis used a Rh target and a 4 kW maximum power setting, and determined the concentrations of a series of elements, including Si, Ti, Al, Fe, Mn, Mg, Ca, Na, K, P, Mn, C, S, Sc, V, Cr, Co, Ni, Cu, Zn, Ga, Ge, As, Se, Rb, Sr, Y, Zr, Nb, Mo, Ag, Sb, Ce, Ba, Nd, Eu, Ho, Er, Yb, Lu, Ta, W, Re, Pt, Au, Hg, Te, Pb, Bi, Th, and U. The analytical procedures used are similar to those outlined in Longerich, 1995 and are summarized here. Prior to analysis, samples were powdered to 30–40 μm using an agate pestle and mortar. Five grams of the resulting powdered sample was then mixed with 10% of Chemplex boric acid before being pressed in a pellet at 25 t (metric) pressure. A pressed pellet approach was used here rather than a fusion disc approach as the latter may result in the loss of volatile elements during high temperature fusion. Semi-quantitative concentrations were determined using a standard-less analytical method. Data acquisition, peak intensity calibration, and element content calculations were undertaken using the Integrated Analytical Intelligence approach within the SPECTRA plus software package, yielding 0.5% uncertainties (Takahashi, 2015).

3.4. XRD analysis

The mineralogies of a total of 50 complete size fraction and whole-rock samples were determined using XRD employing a Bruker D5000 X-ray diffractometer at UQÀM using the approach outlined in Simon et al. (2014). Prior to analysis, individual samples were ground in a mortar to obtain a powder <10 μm in size, and free of any preferential orientation. The powder was then packed in a solid cobalt plate in holders of 5 cm in diameter (X-ray λ: CoKa1: 1.78896). The samples were scanned between 3° and 90° (2θ) at an angle step of 0.02, and with 0.6 sec duration per step. Each analysis lasted 15 min and the resulting diffractogram was analyzed using the EVA software package (DIFFRAC. EVA of the Bruker DIFFRAC.SUITE). The grain size approach allows the determination of quantitative evolution within the minerals in the different sub-samples. Semi-quantitative mineral abundances were calculated using the peak height (in counts per second) of the first diffraction peak for each mineral corrected for quartz and normalized to 100% (Cook et al., 1975). The estimated uncertainty (1σ) of these mineral abundance calculations is 5%.

3.5. Principal component analysis

Principal component analysis can be used to evaluate the variance of a dataset, using a small number of orthogonal variables (principal components), the calculation of eigenvectors, or artificial linear combinations of the original variable (i.e., elements). Each successive principal component accounts for a lesser and decreasing amount of variance. In geochemical data, the majority of variability can be accounted for by the first few principal components, thus reducing the number of dimensions. Each principal component likely reflects an individual process affecting the data, such as alteration and mineralization (Grunsky, 2010).

The geochemical compositions of rocks are considered "closed", because the sum of analytical data is constant (i.e., 100%), and this closure issue results in a lack of independence between variables. This problem was avoided by applying a centered log ratio (CLR) transformation to all data prior to statistical analysis, as suggested by Aitchison (1986). The PCA undertaken during this study utilized the SPSS 16.0 statistical software package (Norusis, 2008), and principal components were extracted using correlation matrixes. Principal component loadings and scores are used to describe the importance of

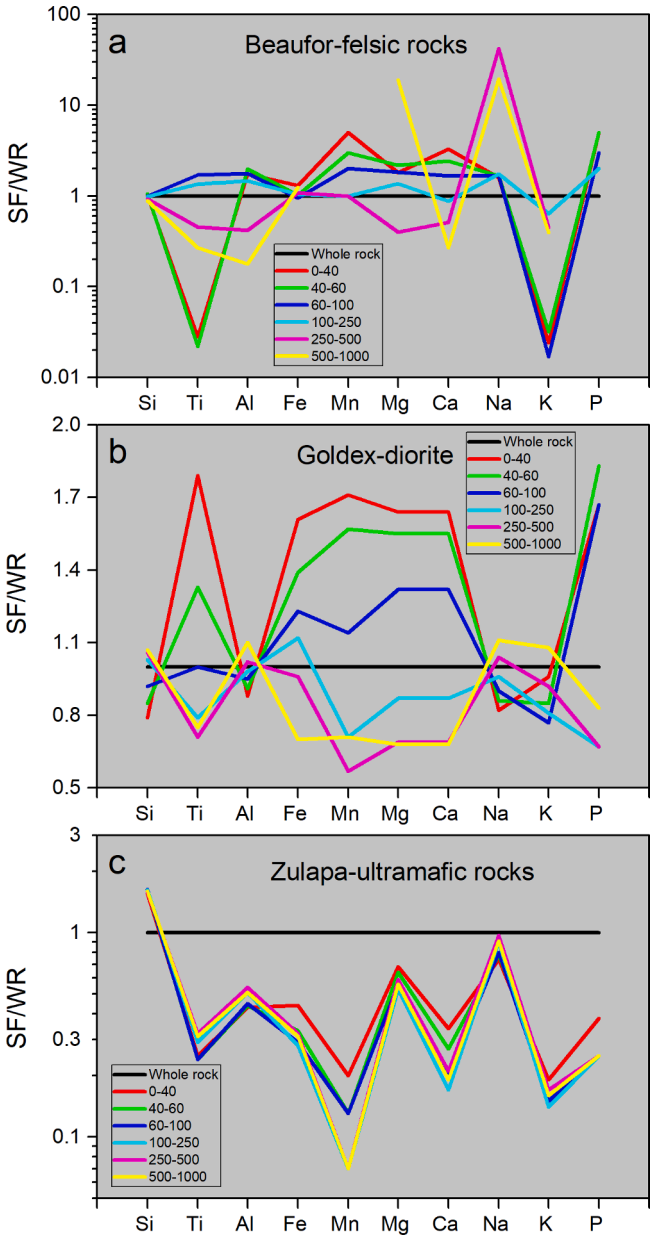

Fig. 3. Variations in major-element (Si, Ti, Al, Fe, Mn, Mg, Ca, Na, K, and P) concentrations within different size fractions (SF), normalized to the concentrations of the same elements within whole-rock (WR) samples for (a) the felsic rock-hosted Beaufor, (b) the diorite-hosted Goldex, and (c) the ultramafic-hosted Zulapa deposits.

variables (i.e., elemental concentrations or mineral abundances) and observations (samples), respectively. The relationship between variables is shown as scatterplots that indicate the loading and score values of pairs of components (e.g., P1–P2). The loadings express how variables can be linearly combined to yield the scores. The magnitude of individual loadings provides information on the impact of a particular element or mineral on sample classification, and variables with loadings outside the –0.5 to 0.5 interval are the most important (Davis, 1986). Elements and minerals that plot in the same quadrant positively and negatively correlate with those within the opposite quadrant. The correlation of elements and minerals in the loading plot determines the sample distribution in the score plot, with the identification of relationships among samples, elements, and minerals facilitated by plotting principal component scores and loadings in the same space. The terms PC_E and PC_M are used to represent principal components based on

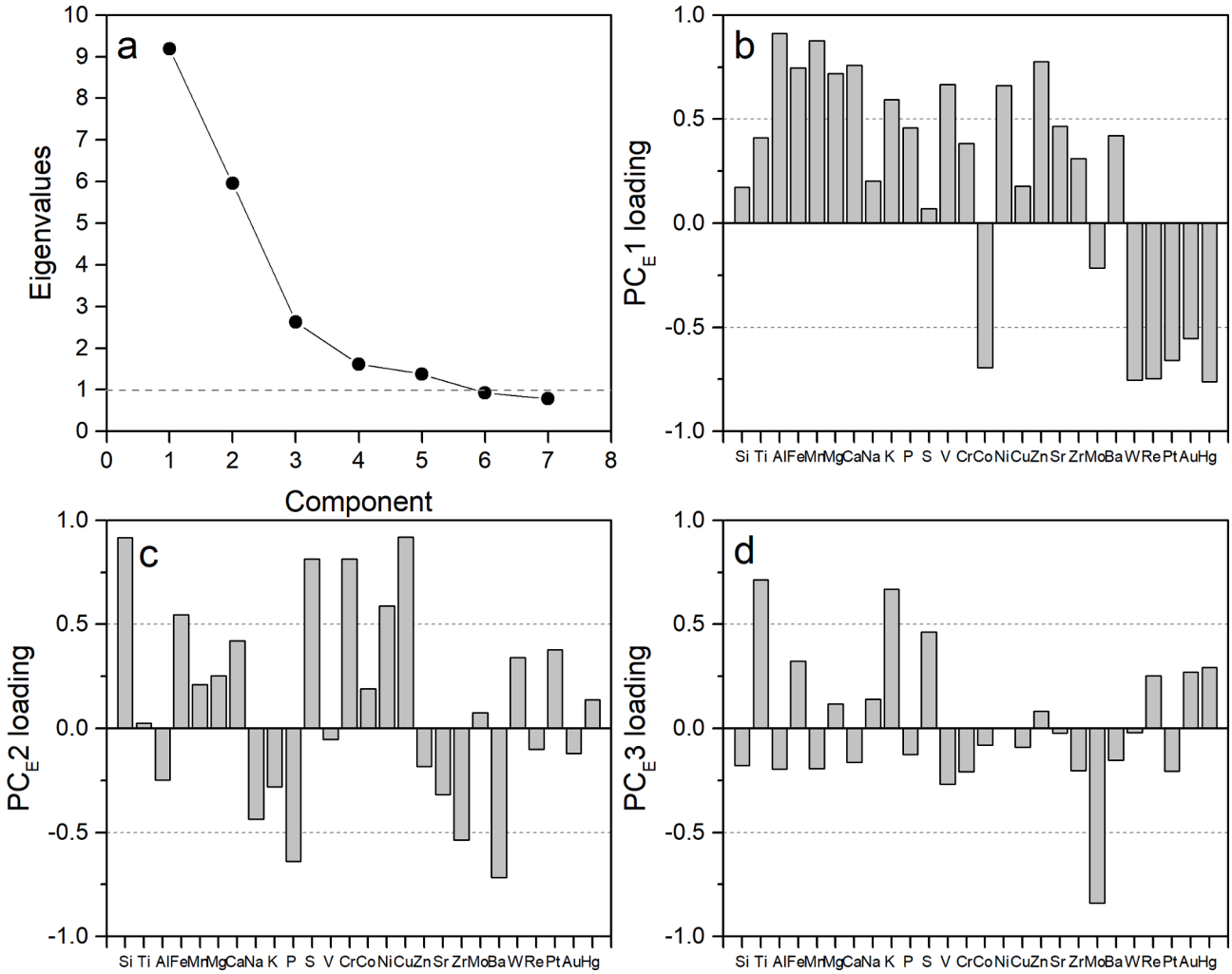

Fig. 4. Results of the PCA of centered log ratio transformed element concentrations within mineralized rocks from orogenic gold deposits in Abitibi. (a) Eigenvalues for seven principal components, the first five of which have eigenvalues larger than one. (b–d) Element loadings for the first three principal components; loadings with absolute values >0.5 are considered statistically meaningful. PC$_E$1 has positive loadings for Al, Fe, Mn, Mg, Ca, K, V, Ni, and Zn, and negative loadings for Co, W, Re, Pt, Au, and Hg, whereas PC$_E$2 positively correlates with Si, Fe, S, Cr, Ni, and Cu, but negatively correlates with P, Zr, and Ba. PC$_E$3 has positive loadings for Ti and K, and negative loadings for Mo.

elemental geochemistry and mineral abundance, respectively.

4. Geochemical approach and results

4.1. Chemical composition of mineralized rocks

The major- and trace-element compositions of the mineralized samples from the study area are given in Appendix A. Variations in the chemical compositions of samples from different deposits can be identified using boxplots (Fig. 2). These samples contain 21–24 wt% Si and 1–10 wt% Al, Fe, Mg, Ca, Na, and K (Fig. 2a–c), with Ti, C, and S contents that range from hundreds of ppm to 8 wt% (Fig. 2a, c), and P, Ni, Cu, and Ba contents ranging from ~100 to ~2000 ppm (Fig. 2c–f). Tungsten concentrations are highly variable (40–7500 ppm; Fig. 2g) with other elements (including V, Cr, Co, Zn, Sr, Zr, Mo, Yb, Ta, Re, Pt, Au, and Hg) present at concentrations lower than ~500 ppm. Comparing samples from different deposits indicate that Si, Fe P, Cr, Ba, Yb, Ta, and Re contents are within one order of magnitude, but other elements have inter-deposit content variations that differ by two or three orders of magnitude (Fig. 2).

The major element concentrations of whole-rock and different size-fraction samples from the Beaufor, Goldex, and Zulapa gold deposits are used to illustrate compositional variations with changes in size fraction. These three deposits have different host rocks that range in composition from felsic to mafic–ultramafic. The size-fraction data for deposits with different host rocks are plotted in whole-rock concentration-normalized variation diagrams (Fig. 3) that indicate that the smaller size-fraction (i.e., 0–40, 40–60, and 60–100 μm) samples from the Beaufor deposit are depleted in K and Ti, relative to whole-rock concentrations, whereas larger size fractions (i.e., 200–500 and 500–1000 μm) are relatively enriched in Na (Fig. 3a). In comparison, smaller size-fraction samples (i.e., 0–40, 40–60, and 60–100 μm) from the Goldex deposit have major element concentrations that contrast significantly with those in the larger size-fraction samples (i.e., 100–250, 250–500, and 500–1000 μm), with the 0–100 μm sample containing relatively high concentrations of Ti, Fe, Mn, Mg, Ca, P, and low concentrations of Si, Al, Na, and K. All size fraction samples from the Zulapa deposit have similar relatively depleted patterns, barring Si, compared with their whole-rock concentrations.

4.2. PCA results

Five principal components with eigenvalues >1 were extracted from all of the XRF data used during this study (Fig. 4a), accounting for 35%, 23%, 10%, 6%, and 5% of the variance in the dataset. The first three principal components (PC$_E$1, PC$_E$2, and PC$_E$3) account for a total of 68%

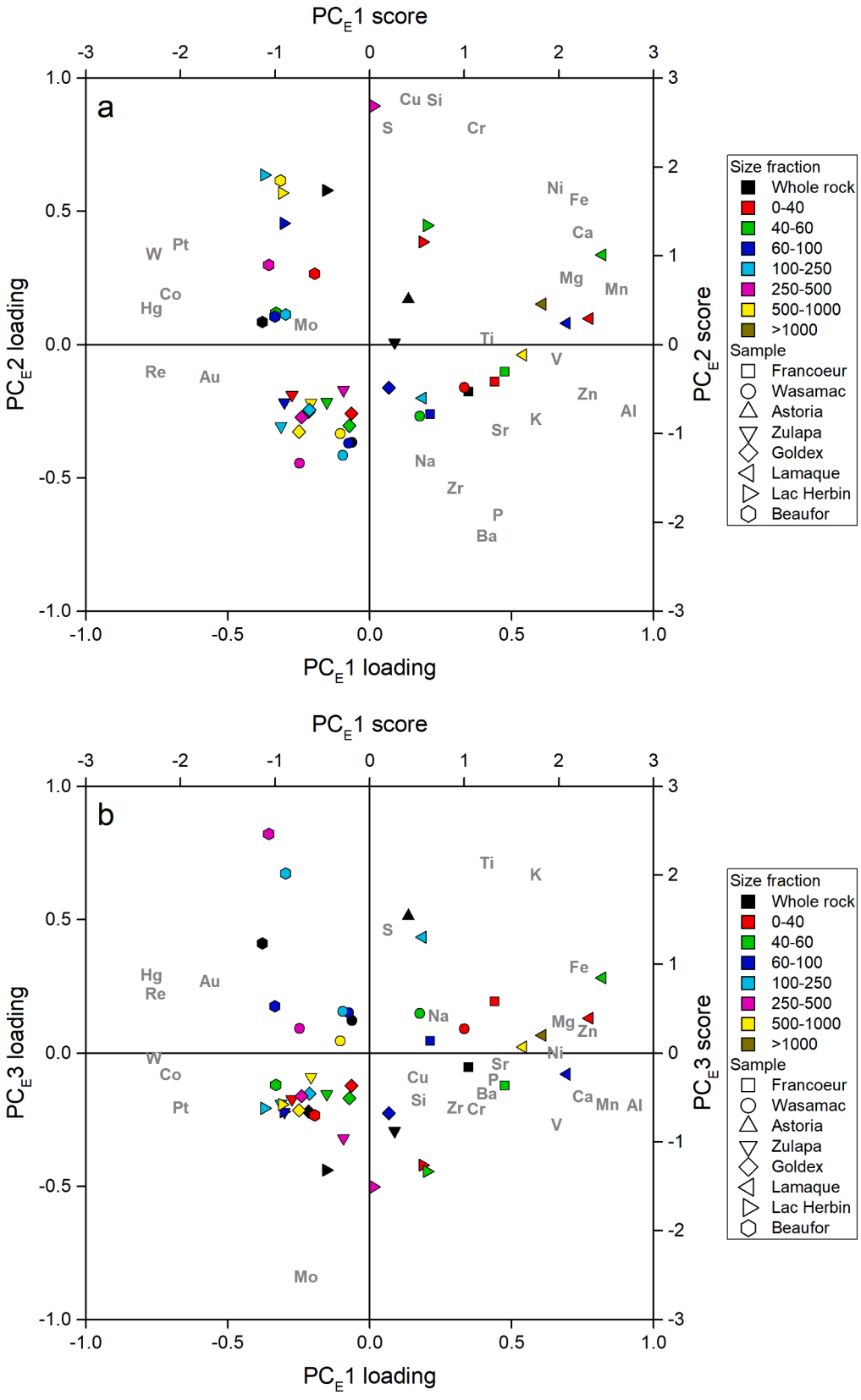

Fig. 5. Results of the PCA of elemental concentrations within ore-bearing rocks from the Francoeur, Wasamac, Astoria, Zulapa, Goldex, Lamaque, Lac Herbin, and Beaufor orogenic gold deposits of the Abitibi greenstone belt. These data are displayed as compositional biplots showing principal component scores for all analyses (samples) and principal component loadings for individual variables (elements). The x- and y-axes in both (a) and (b) correspond to the gray element labels, whereas the right and top axes correspond to the color-filled symbols for different samples. (a) Diagram showing variations in PC_E1 vs. PC_E2 values showing the separation of ore-forming (Pt, W, Co, Hg, Re, Au) and lithological (e.g., Fe, Ca, Mn, Mg, Al, K) elements. (b) Diagram showing variations in PC_E1 vs. PC_E3 values showing the separation of Ti and K from Mo.

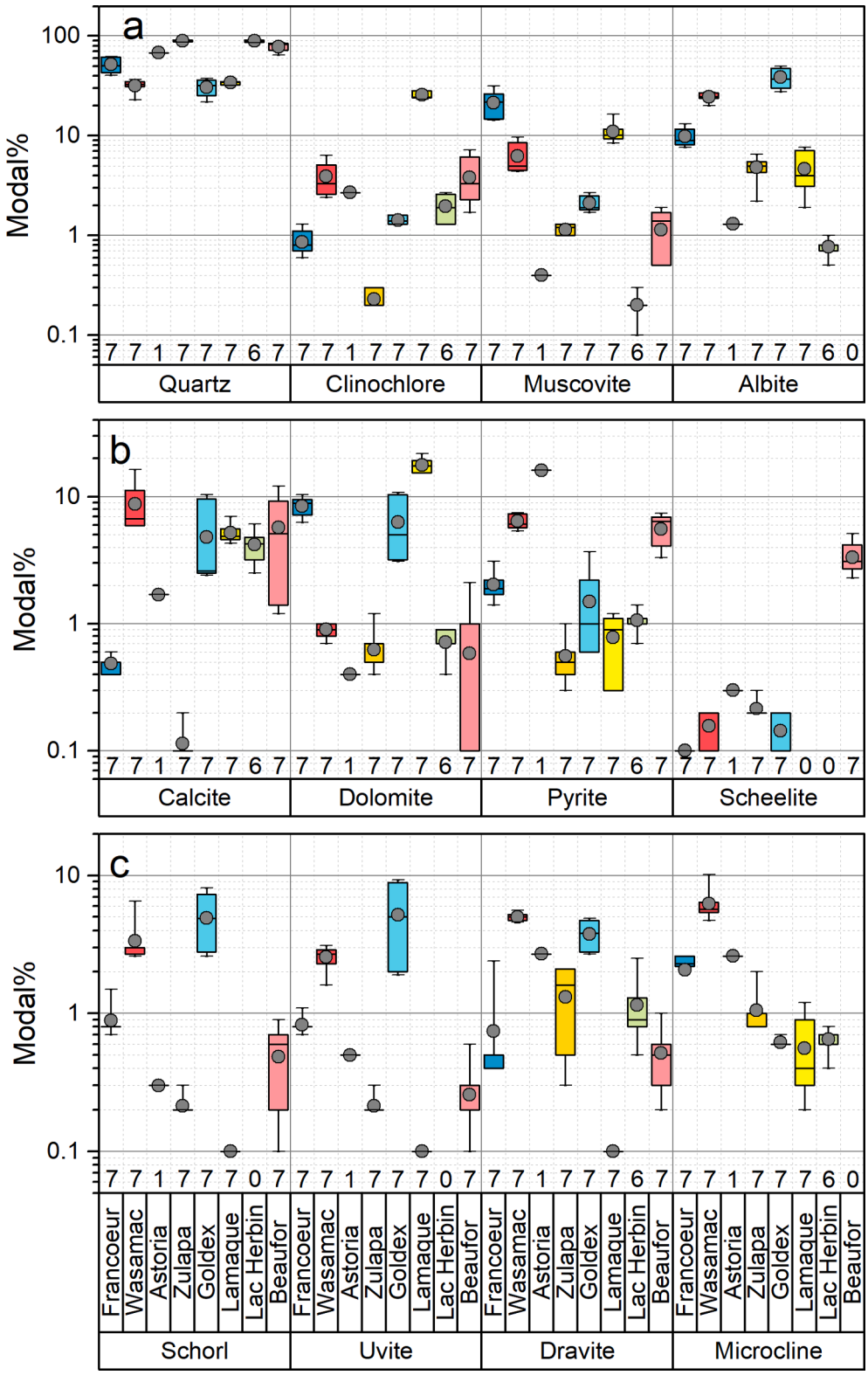

Fig. 6. Box and whisker plots showing variations in the mineralogical composition of mineralized rocks from orogenic gold deposits of Abitibi. The different components within this diagram are similar to those described for Fig. 2 with the number along the x-axis indicating the number of analyses for each deposit.

of this variance, and form the focus of this discussion. Element loadings for principal components that have absolute values >0.5 are considered statistically meaningful (Fig. 4b–d), and the relationship between loadings and scores is shown in PC_E1–PC_E2 and PC_E1–PC_E3 diagrams in Fig. 5.

The PC_E1 component has positive Al, Fe, Mn, Mg, Ca, K, V, Ni, and Zn, and negative Pt, W, Co, Hg, Re, and Au loadings (Figs. 4b and 5a), whereas PC_E2 is characterized by positive loadings for Cu, S, Si, Cr, Ni, and Fe, and negative loadings for Zr, P, and Ba (Figs. 4c and 5a). The PC_E3 component has positive loadings for Ti and K, and negative loadings for Mo (Fig. 4d and 5b). Despite having lower absolute loadings, PC_E3 also positively correlates with Au, Re, and Hg, and negatively

correlates with Co, Pt, and Mo (Figs. 4d and 5b).

We define an element mineralization index (EMI) using PC_E1 combined with element concentrations and their absolute loadings as follows: EMI = Σ(C(*X*)*AL(*X*))/Σ(C(*Y*)*AL(*Y*)), where C(*X*) represents the content of element *X* , AL(*X*) represents the absolute loading of element *X* , *X* includes the ore-related elements Co, W, Re, Pt, Au, and Hg, and *Y* includes the rock-forming elements Al, Fe, Mn, Mg, Ca, K, V, Ni, and Zn. The EMI values for samples from the Francoeur, Wasamac, Astoria, Zulapa, Goldex, Lamaque, Lac Herbin, and Beaufor deposits are 0.2–0.5, 0.2–2.3, 1.0, 5.1–18.5, 1.0–2.4, 0.2–1.7, 0.8–46.4, and 24.5–69.6, respectively (Appendix A).

Samples from the Lac Herbin, Beaufor, Zulapa, Goldex, and Wasamac deposits generally have negative PC_E1 values that indicate higher concentrations of W, Pt, Hg, Co, and Mo (Fig. 5a), whereas samples from the other deposits are characterized by higher concentrations of lithological elements such as Ni, Fe, Ca, Mg, Mn, V, K, Zn, and Al (Fig. 5a). Some samples from the Lac Herbin deposit contain elevated concentrations of Cu, S, Si, and Cr, whereas some samples from the Francoeur deposit contain higher concentrations of Zr, P, and Ba (Fig. 5a), compared with the other deposits. In addition, some samples from the Lac Herbin deposit are enriched in Mo, whereas some samples from the Beaufor deposit contain elevated Ti and K concentrations (Fig. 5b).

The influence of size fractions on elemental PCA values can be evaluated by analysis of the distribution of different size fractions from the same sample or deposit. The whole-rock and size-fraction data for the Francoeur, Goldex, and Beaufor deposits cluster in specific quadrants (i.e., the positive PC_E1–negative PC_E2, negative PC_E1–negative PC_E2, and negative PC_E1–positive PC_E2 regions, respectively; Fig. 5a). The fact that whole-rock and size-fraction data for the same deposit cluster in the same quadrant indicate that the results of the PCA undertaken in this study are not influenced by size-fraction variations. Whole-rock and size-fraction samples from the Wasamac and Lac Herbin deposits have negative and positive PC_E2 scores, respectively, whereas those from the Lamaque deposit have positive PC_E1 scores. The fact that these different size fractions from the same deposit have consistent negative or positive scores for specific principal components also indicates that size fractions have little influence on the results of PCA. Finally, the whole-rock sample from the Zulapa deposit plots on a line with a PC_E2 score of zero, but has a PC_E1 score of ~0.1 (Fig. 5a), indicating that the whole-rock data is not important for PCA regression. Different size fractions for the Zulapa sample also cluster in the same negative PC_E1 and PC_E2 quadrant, again consistent with size-fraction variations and sample preparation having little influence on the results of PCA.

5. Mineralogical approach and results

5.1. Mineral abundance variations between deposits

Boxplots were used to identify the main differences in mineral abundance among different deposits (Fig. 6). All of the samples are dominated by quartz (21.8%–93.6% abundance; Fig. 6a) with clinochlore, muscovite, albite, calcite, dolomite, and pyrite abundances varying between 0.1% and ~50% (Fig. 6a, b), and scheelite, schorl, uvite, dravite, and microcline abundances generally <10% (Fig. 6b, c). Samples from the Francoeur deposit have relatively high dolomite and muscovite abundances, whereas the Wasamac samples have elevated abundances of albite, microcline, calcite, schorl, uvite, and dravite (Fig. 6). The Astoria samples have higher pyrite abundances, whereas the Beaufor samples contain more scheelite (Fig. 6). Finally, samples from the Goldex deposit have higher albite, schorl, uvite, and dravite abundances (Fig. 6).

The effect of size-fraction variations on mineral abundances was investigated by normalizing mineral abundances for different size fractions to the mineral abundances obtained for the whole-rock aliquot of the same sample. Samples with different host rocks have different

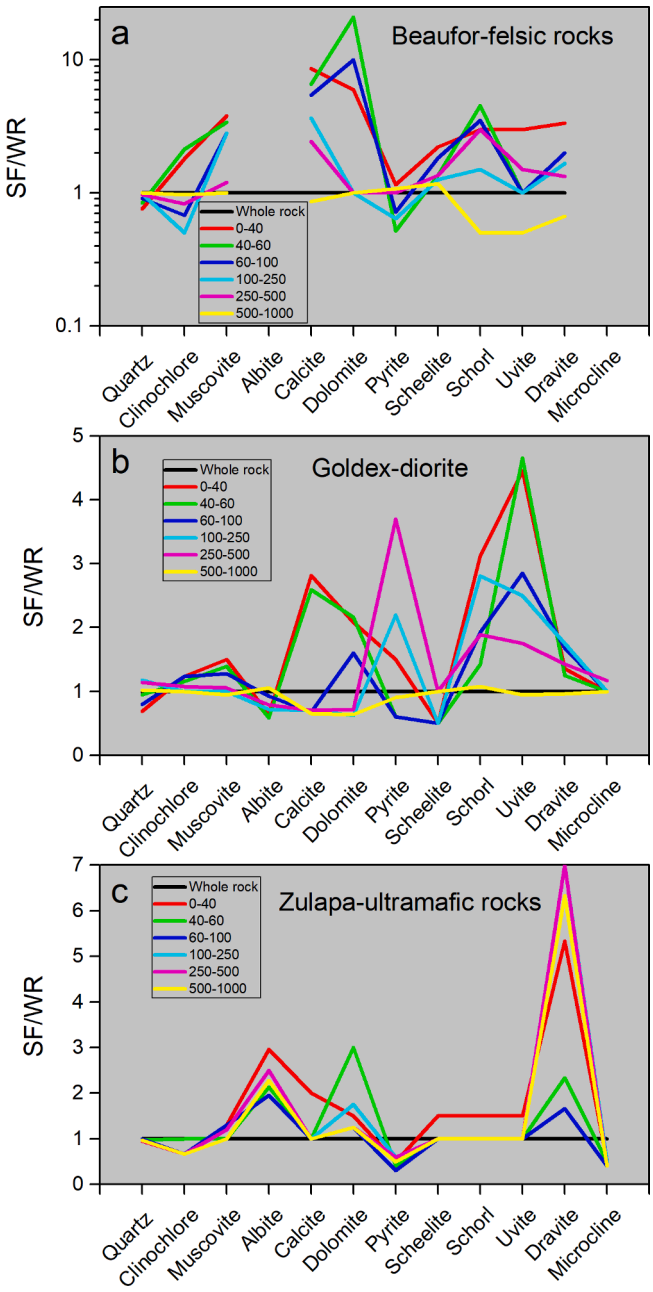

Fig. 7. Mineral abundances within different size fractions (SF) normalized to the abundances within whole-rock (WR) samples within (a) the felsic-hosted and albite-free Beaufor deposit, (b) the diorite-hosted Goldex deposit, and (c) the ultramafic-hosted Zulapa deposit.

normalization patterns (Fig. 7), with the felsic-hosted Beaufor deposit having clinochlore depletions in the 60–100, 100–250, and 250–500 μm size fractions, pyrite depletions in the 40–60, 60–100, and 100–250 μm size fractions, and schorl, uvite, and dravite depletions in the 500–1000 μm size fraction (Fig. 7a). Size fraction data from the diorite-hosted Goldex deposit indicate that size fractions below 500 μm are depleted in albite, 60–1000 μm size fractions are relatively depleted in calcite and dolomite compared with the <60 μm size fraction, and size fractions <250 μm are relatively depleted in scheelite in contrast with the >250 μm size fractions (Fig. 7b). Finally, different size fractions from the ultramafic-hosted Zulapa deposit all have similar normalized patterns that are relatively depleted in clinochlore, pyrite, and microcline, but enriched in other minerals (Fig. 7c).

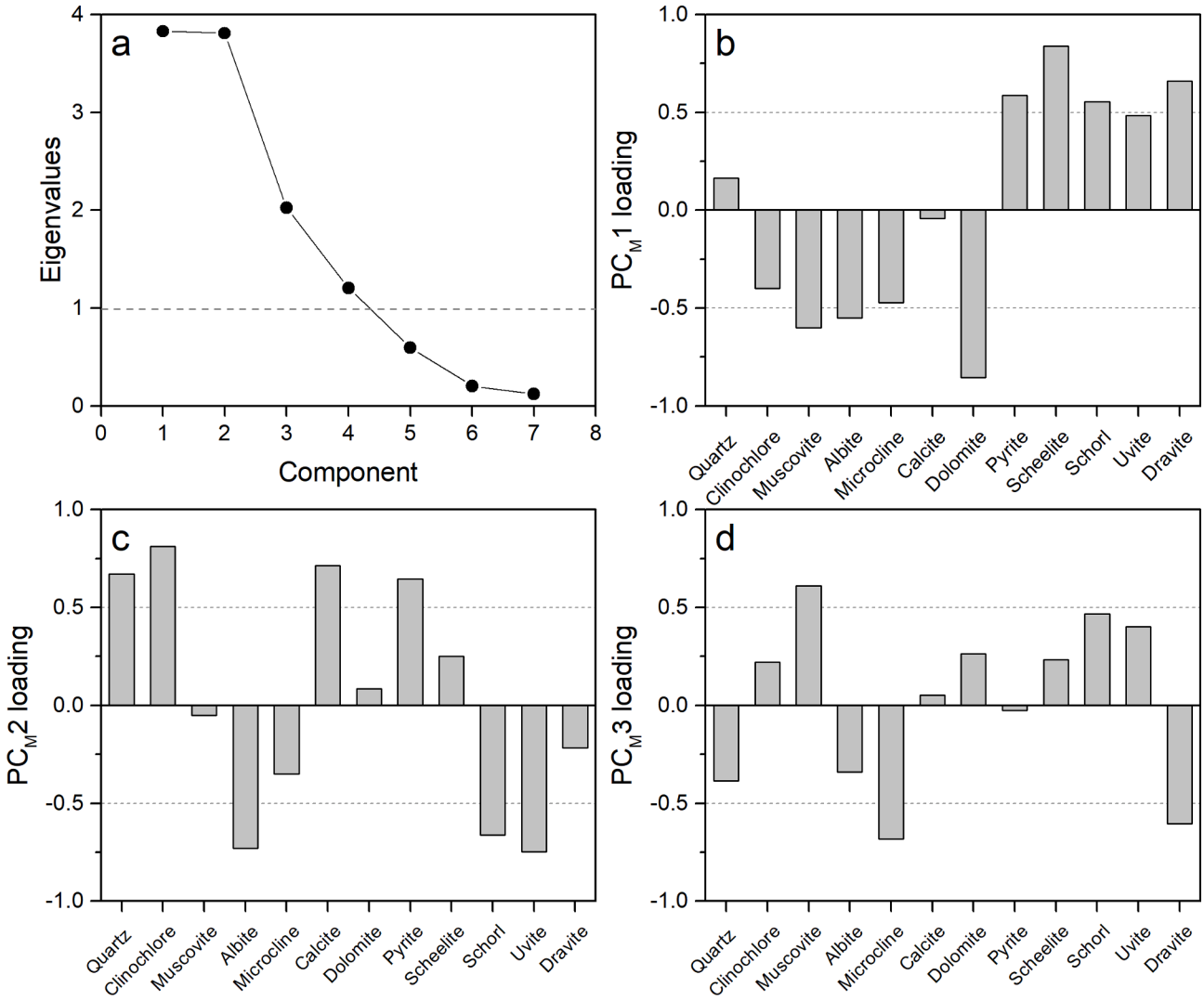

Fig. 8. Results of the PCA of centered log ratio-transformed mineralogical abundances of mineralized rocks from orogenic gold deposits within Abitibi. (a) Eigenvalues for seven principal components, the first four of which have eigenvalues >1. (b–d) Element loadings for the first three principal components, where loadings with absolute values >0.5 are considered statistically meaningful. PC_M1 has positive loadings for pyrite, scheelite, schorl, uvite, and dravite, and negative loadings for muscovite, albite, and dolomite, whereas PC_M2 positively correlates with quartz, clinochlore, calcite, and pyrite, but negatively correlates with albite, schorl, and uvite, and PC_M3 has positive loadings for muscovite but negative loadings for microcline and dravite.

5.2. PCA results

Only four of the mineral-related principal components determined during this study are statistically meaningful because they have eigenvalues larger than one (Fig. 8a). We consider the first three principal components (PC_M1, PC_M2, and PC_M3) that account for 32%, 32%, and 17% of the variance within the dataset, respectively. The mineral loadings for individual principal components are shown in Fig. 8b–d and are plotted along with scores in PC_M1–PC_M2 and PC_M1–PC_M3 spaces in Fig. 9a and b.

PC_M1 has negative loadings for muscovite, albite, and dolomite, and positive loadings for pyrite, scheelite, schorl, uvite, and dravite (Figs. 8b and 9a), indicating that this principal component separates alteration minerals rich in Ca, Na, and K from ore-related minerals. Pyrite, scheelite, and tourmaline are all important indicators of orogenic gold mineralization, with PC_M2 having negative loadings for albite, schorl, and uvite, and positive loadings for quartz, clinochlore, calcite, and pyrite (Figs. 8c and 9a). This suggests that PC_M2 can separate different types of vein (e.g., tourmaline veins versus quartz–calcite–pyrite veins). PC_M3 correlates positively with muscovite, schorl, and uvite and correlates negatively with microcline, dravite, and albite (Figs. 8d and 9b).

Here we define a mineral mineralization index (MMI) based on mineral abundances and their absolute loadings within the PC_M1 principal component as follows: $EMI = \Sigma(A(X)^*AL(X))/\Sigma(A(Y)^*AL(Y))$, where $A(X)$ represents the abundance of mineral X , and $AL(X)$ represents the absolute loading of the same mineral X. Minerals are divided into X , which includes ore-related minerals such as pyrite, scheelite, schorl, uvite, and dravite, and Y, which includes alteration minerals such as muscovite, dolomite, albite, and microcline. The MMI values for samples from the Francoeur, Wasamac, Astoria, Zulapa, Goldex, Lamaque, Lac Herbin, and Beaufor deposits are 0.07–0.17, 0.42–0.54, 4.74, 0.22–0.47, 0.16–0.49, 0.01–0.04, 0.90–1.55, and 1.97–17.1, respectively (Appendix B).

Samples were separated into four groups in PC_M1–PC_M2 space, reflecting variations in mineral assemblages. Samples from the Lamaque and Lac Herbin deposits are characterized by a mineral assemblage dominated by clinochlore, calcite, and dolomite, whereas samples from Beaufor and Astoria contain more quartz, pyrite, and scheelite (Fig. 9a). Samples from the Francoeur deposit also have relatively high muscovite, microcline, and albite abundances, whereas samples from the Wasamac, Zulapa, and Goldex deposits contain more tourmaline (i.e., uvite, schorl, and dravite; Fig. 9a). The Lamaque, Beaufor, and Lac Herbin deposits

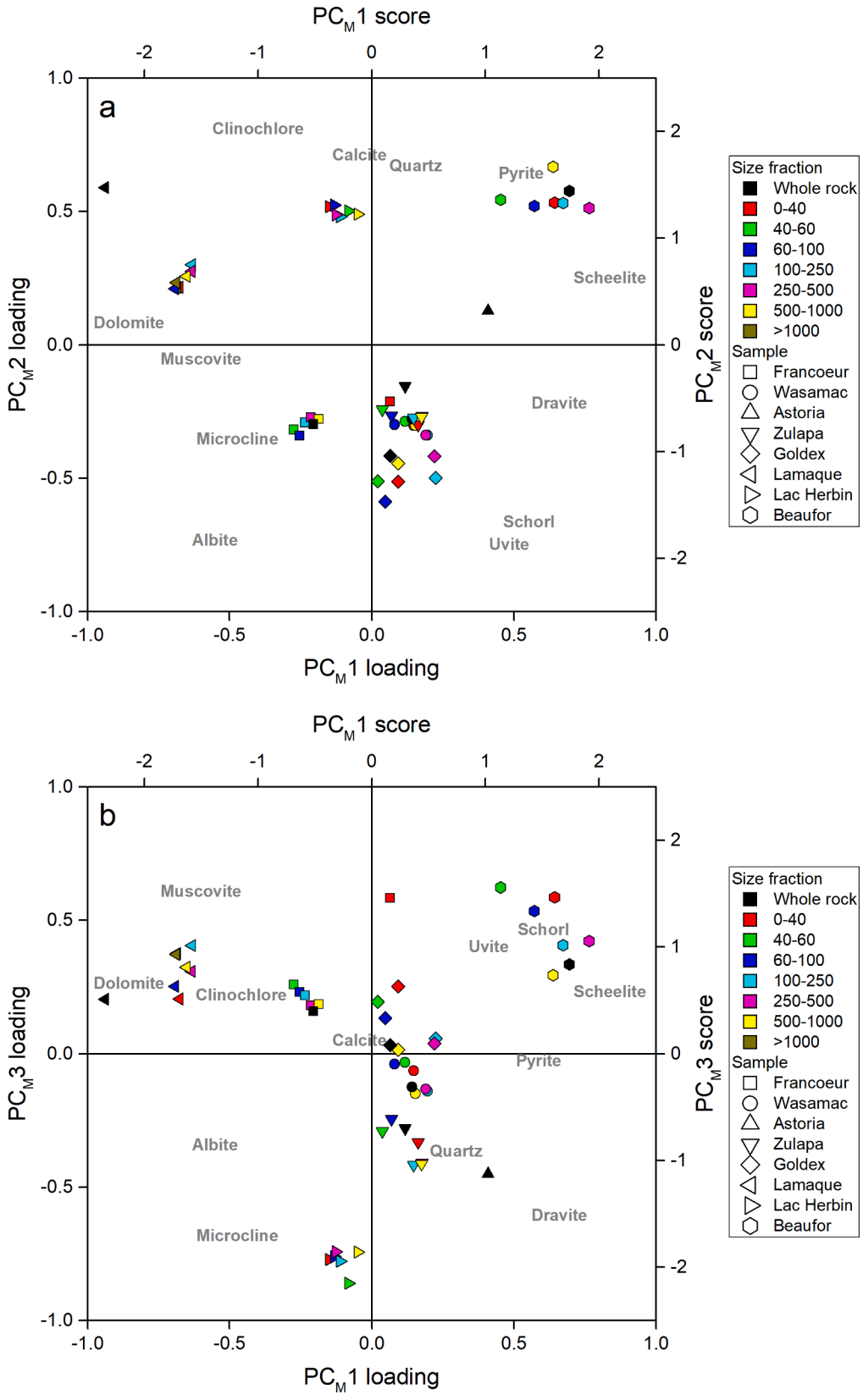

Fig. 9. Results of the PCA of XRD data for ore-bearing rocks from eight orogenic gold deposits within the Abitibi greenstone belt, shown as compositional biplots showing principal component scores for all analyses (samples) and principal component loadings for variables (minerals). The left and bottom axes in (a) and (b) correspond to the gray mineral labels whereas right and top axes correspond to color-filled symbols for different samples. (a) Diagram showing variations in PC_M1 vs. PC_M2 values indicating the separation of ore-related minerals (pyrite, scheelite, dravite, schorl, and uvite) from rock-forming minerals (clinochlore, dolomite, muscovite, microcline, and albite). (b) Diagram showing variations in PC_M1 vs. PC_M3 showing the separation of muscovite from microcline and dravite.

Table 2
Comparison between different classification methods.

Method	Geochemical classification			Mineralogical classification		
	Positive loading	Negative loading	Interpretation	Positive loading	Negative loading	Interpretation
PC1	Al, Fe, Mn, Mg, Ca, K, V, Ni, Zn	Pt, W, Co, Hg, Re, Au	PC_E1 separates ore-related elements from rock-forming elements, thus discriminating mineralization from barren rocks	Pyrite, scheelite, tourmaline, schorl, uvite, dravite	Muscovite, albite, dolomite	PC_M1 discriminates altered rocks from mineralization
PC2	Cu, S, Si, Cr, Ni, Fe	Zr, P, Ba	PC_E2 separates elements constituting ore minerals such as pyrite, chalcopyrite, pyrrhotite, and alteration mineral such as fuchsite from elements of igneous accessory minerals	Quartz, clinochlore, calcite, pyrite	Albite, schorl, uvite	PC_M2 discriminates minerals comprising different types of veins/ alteration
PC3	Ti, K (Re, Au, and Hg with lower loadings)	Mo (Pt and Co with lower absolute loadings)	PC_E3 separates K-Fe alteration from molybdenite. PC_E3 may also distinguish orogenic fluids from magmatic influence	Muscovite	Microcline, dravite	PC_M3 may distinguish different alteration parageneses

Note: PC_E1, PC_E2, and PC_E3 represent the first, second, and third principal components of geochemical classification method, respectively. PC_M1, PC_M2, and PC_M3 represent the first three principal components of mineralogical classification method.

also plot separately from the other deposits in a PC_M1 vs. PC_M3 diagram (Fig. 9b). This reflects the fact that samples from the Lamaque deposit contain more muscovite, dolomite, and clinochlore, relative to other deposits, whereas samples from the Beaufor deposit have relatively high uvite, schorl, and scheelite abundances (Fig. 9b). Samples from the Lac Herbin deposit also contain more microcline and dravite than other deposits (Fig. 9b). Different size-fraction samples from the same deposit have mineral abundance related PCA values that cluster together and plot in the same quadrant (Fig. 9a, b), indicating that size-fraction differences have no impact on mineral-based PCA values. This is true for the Lamaque deposit, despite the whole-rock sample potting separately from the size-fraction samples from the same deposit, because all of these samples plot in the same quadrant (Fig. 9a). This means that differences in mineral abundances between whole-rock and size-fraction data do not affect the PCA analysis of samples from the Lamaque deposit, again consistent with size-fraction variations having little influence on mineral abundance-based PCA.

6. Discussion

6.1. Comparison between different classification methods

Different classification methods can provide different information on host rocks, alteration, and mineralization. Table 2 compares the three principal components derived from the geochemical and mineral classification methods used during this study. Here, PC_E1 separates rock-forming (Al, Fe, Mn, Mg, Ca, K, V, Ni, and Zn) and hydrothermal/ore-related elements (Pt, W, Co, Hg, Re, and Au), indicating that PC_E1 is a very efficient discriminator between mineralized and barren host rocks, with the latter either altered or unaltered, but generally lacking in mineralization. In addition, PC_M1 separates alteration minerals rich in Ca, Na, and K from Fe or W-rich ore minerals such as pyrite, tourmaline, and scheelite, therefore providing a discriminant between altered host rocks and mineralization. This indicates that both PC_E1 and PC_M1 can efficiently discriminate between mineralization and barren rocks.

The PC_E2 component separates ore elements (e.g., Cu–S–Fe in chalcopyrite, Fe–Ni in pyrite or pyrrhotite, and Si–Cr in fuchsite) from alteration elements (Si from quartz), and from rock-forming elements (Zr from zircon, P from apatite, and Ba–[K–Sr] from K-feldspar), indicating that PC_E2 can efficiently discriminate between mineralization and altered host rocks. The PC_M2 component separates Si-rich minerals, such as quartz, from low Si minerals, such as albite, uvite, and schorl, indicating that this component can discriminate between different types of mineralization (e.g., disseminated vs. vein-hosted mineralization). This indicates that the PC_E2 and PC_M2 components provide different information, where PC_E2 discriminates between altered and unaltered host rocks, indicating that it represents a useful tool for characterizing host rock alteration, whereas PC_M2 discriminates between disseminated and vein-hosted mineralization, meaning that it is useful for distinguishing between mineralization types.

The information extracted from the PC_E3 and PC_M3 components is not as clear as those extracted from their respective first and second principal components. The PC_E3 component separates K–Fe alteration (K from potassic minerals, Ti from Fe–Ti oxides) from molybdenite; Mo). The PC_E3 component also separates the ore elements Re, Au, Hg, and W from Mo, Pt, and Co. The platinum group elements (including Pt, Pd, Rh, Os, Ir, and Ru) are commonly enriched in mafic–ultramafic rocks and related magmatic Ni–Cu sulfide deposits (Naldrett, 2004), whereas Co and Ni are generally enriched in pyrite from magmatic Ni–Cu sulfide deposits and magmatic–hydrothermal deposits, such as porphyry Cu and iron oxide–copper–gold deposits (e.g., Bajwah et al., 1987; Meng et al., 2019). Element assemblages enriched in Pt, Co, and Mo are therefore indicative of possible magmatic contributions as a result of fluids being exsolved from mafic magmas or fluids altering and replacing mafic–ultramafic rocks. The positive loadings for Ti, K, Re, Au, and Hg suggest that the main ore element Au (as well as Re and Hg) may be related to K–Fe alteration. This means that the PC_E3 component can be used to discriminate between different fluid and mineralizing processes (e.g., truly orogenic mineralization vs. deposits influenced by magmatism). In comparison, PC_M3 may distinguish between different alteration paragenesis, such as albite + microcline vs. uvite and schorl. This means that the PC_E3 and PC_M3 components can provide more complex information relating to mineralization and alteration, and may also provide insights into hydrothermal fluid compositions.

In summary, both PC_E1 and PC_M1 can similarly discriminate between mineralized and altered or unaltered barren rocks, whereasPC_E2 and PC_M2 provide more detailed information on alteration and mineralization, respectively. Finally, PC_E3 and PC_M3 may provide information on the different compositions of fluids responsible for the mineralization and alteration in an area.

6.2. Implications for mineral exploration

Multivariate statistical methods such as PCA have been widely used to characterize the alteration and mineralogy of mineralized systems, and to identify sources of metals and fluids, all of which indicate their potential applications for mineral exploration (Chandrajith et al., 2001; Crosta et al., 2003; Grunsky, 2010; Cheng et al., 2011; Makvandi et al., 2016; Meng et al., 2017; Chen et al., 2018). For example, the PCA of the chemical composition of stream sediments in the Walawe Ganga Basin of Sri Lanka led Chandrajith et al. (2001) to determine that areas that contain calc-silicate/marble and charnockitic rocks are probable source regions for certain minerals, particularly in the axial regions of anticlines. Chen et al. (2011) also used a distance-based fuzzy mask in

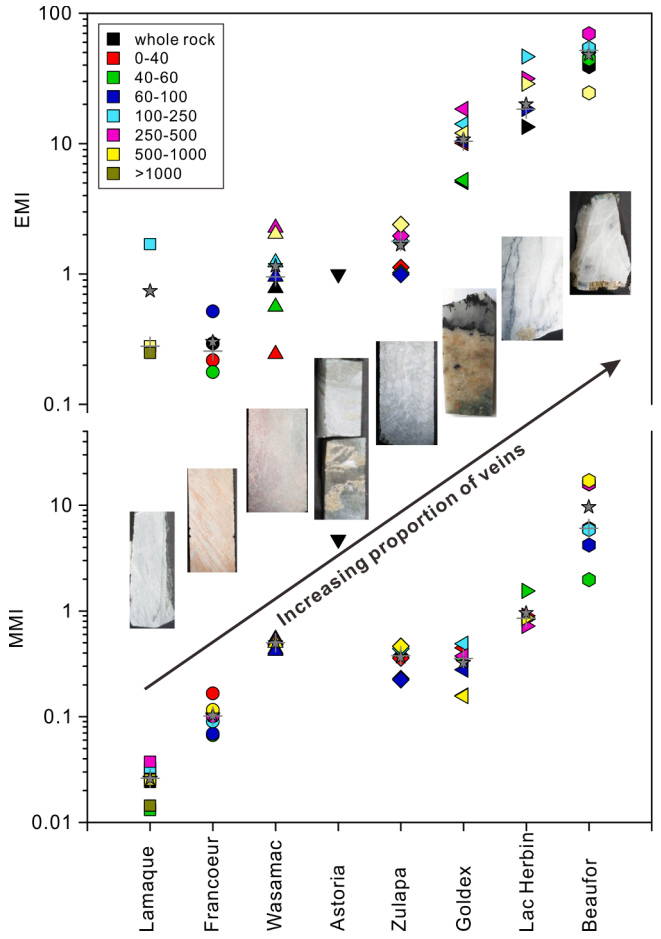

Fig. 10. Diagram showing variations in element mineralization index (EMI) and mineral mineralization index (MMI) values for different gold deposits in the study area where EMI = (C(Co)*0.69 + C(W)*0.75 + C(Re)*0.75 + C(Pt)*0.66 + C(Au)*0.55 + C(Hg)*0.76)/(C(Al)*0.91 + C(Fe)*0.75 + C(Mn)*0.88 + C(Mg)*0.72 + C(Ca)*0.76 + C(K)*0.59 + C(V)*0.67 + C(Ni)*0.66 + C(Zn)*0.78)*1000 and MMI = (C(pyrite)*0.59 + C(scheelite)*0.84 + C(schorl)*0.55 + C(uvite)*0.48 + C(dravite)*0.66)/(C(muscovite)*0.60 + C(dolomite)*0.85 + C(albite)*0.55 + C(microcline)*0.47). Legends indicate variations in size fractions in μm with grey filled stars and crosses indicating the mean and median values for each deposit, respectively. Vein abundances increase from the Lamaque, Francoeur, Wasamac, and Astoria deposits to the Zulapa, Goldex, Lac Herbin, and Beaufor deposits, consistent with the changing textures of the hand specimens from these deposits. Different size fractions from the same deposit have different EMI and MMI values but these variations as a result of changes in size do not influence the overall variations and trends between the deposits. The higher EMI value for the 100–250 μm size fraction from the Lamaque deposit relative to the other size fractions from this deposit reflects the higher Au content of this size fraction.

conjunction with PCA to delineate potential areas for new felsic intrusions (including buried intrusions) and related Sn mineralization in the Gejiu mineral district of Yunnan, China. Finally, Chen et al. (2018) used PCA of geochemical data for sandstones overlying the Phoenix uranium deposit within the Athabasca Basin of Canada to determine that the uranium within the deposit was derived predominantly from basement fluids rather than detrital heavy minerals.

The PCA of geochemical and mineral abundance data for ores from gold deposits within the Abitibi of Canada provides useful information on the mineralization and alteration within these deposits. The most critical first principal components (PC_E1 and PC_M1) can efficiently discriminate between mineralized and barren or altered rocks. The PCA methods outlined in this study allow the quick identification of minerals related to mineralization and those that are not, despite the challenges posed by limited sampling. This approach would be especially useful for greenfields exploration in new areas, and would provide key information on which minerals are associated with mineralization. The PCA method also enables the quantification of the association between minerals and geochemical data, instead of the typically qualitative approach used in the field and during exploration. This quantitative and rapid identification of mineralization and alteration will be particularly useful during mineral exploration in poorly exposed areas (e.g., glaciated regions) where geological fieldwork and exploration may be challenging

The element and mineral mineralization indexes (EMI and MMI) defined during this study can be used to evaluate the intensity of gold mineralization (i.e., the concentrations of elements, or the abundance of minerals associated with gold mineralization vs. values typical for barren or altered host rocks). These indexes were compared with gold grades and textures present in hand specimens from each deposit to assess the feasibility of using PCA-based approaches in mineral exploration. No obvious correlation between EMI or MMI values and variations in deposit gold grade or amount of contained gold was evident, indicating that mineralization intensity at a hand-specimen scale cannot provide an indication of the average gold grade of an entire deposit, primarily as a result of limited sampling. However, EMI or MMI values can provide information on the style of mineralization present in the samples analyzed during this study (e.g., disseminated vs. vein-hosted mineralization), and reflect the relative abundance of pyrite in the samples. The EMI and MMI values calculated during this study increase from the Lamaque deposit through the Francoeur, Wasamac, Astoria, Zulapa, Goldex, and Lac Herbin deposits to the Beaufor deposit, which has the highest values (Fig. 10). This is consistent with variations in mineralization type, from disseminated ores with relatively low sulfide abundances within the Lamaque, Francoeur and Wasamac deposits, to vein-hosted mineralization with increased sulfide abundances in the Goldex, Lac Herbin, and Beaufor deposits. This indicates that use of EMI and MMI with unknown samples can provide information on the likely mineralization intensity and style that is present in an area; this information is essential for gold exploration.

In addition to PC_E1 and PC_M1, the second most important principal components, namely PC_E2 and PC_M2, can also constrain the nature of the host rocks (altered vs. unaltered) and the style of mineralization (disseminated vs. vein) in an area, respectively. This means that PC_E2 values are useful for the identification of altered regions that could host mineralization, whereas PC_M2 values characterize the nature of the mineralization that is likely to be present in an area, providing information that is useful during field-based exploration. The less important third-principal components cannot be used directly during mineral exploration, but instead provide constraints on the nature of ore-forming fluids associated with mineralization in an area, providing insights for future research. In summary, the two geochemistry- and mineralogy-based automatic classification methods developed during this study are complementary, meaning that using both together may well be a useful approach for mineral exploration.

6.3. *Future developments in PCA-based approaches for mineral exploration*

This study has demonstrated that PCA can effectively discriminate between mineralized and barren rocks associated with gold mineralization in the Abitibi Province using geochemical and/or mineral abundance data. However, the limited number of samples used means that the principal components developed during this study that provide information on mineralization, alteration and wall rock characteristics need to be refined using a larger dataset. This also applies to the proposed mineralization indexes (EMI and MMI), which need to be verified by comparing different types of samples from a single deposit to assess the variability of these indices at a deposit scale. Using PCA on a single deposit means that PC_E1 or PC_M1 scores can be used to determine

relative mineralization intensities for individual samples. For example, more negative PC_E1 and more positive PC_M1 scores are likely to represent samples that contain increasing amounts of mineralization. Using PCA approaches in regional mineral exploration should ideally utilize discrimination diagrams that are constructed using known samples (e.g., Makvandi et al., 2016). These sample types can include barren host (e.g., volcanic, sedimentary, and metamorphic rocks), altered (e.g., sodic, potassic, or calcic alteration), and mineralized (e.g., containing different types of mineralization) rocks. The development of PCA-based discrimination diagrams means the origins of unknowns can be determined, indicating the usefulness of PCA approaches using geochemical and mineral abundance data for exploration targeting in greenfield environments, as well as to potentially develop vectors toward mineralization.

7. Conclusions

A detailed geochemical and mineralogical study of eight gold deposits along the CLLFZ combined with PCA of the resulting data has yielded important constraints on the types of mineralization and alteration present within these gold deposits. The PCA-based mineralogical and geochemical classification methods are equally efficient in terms of discriminating mineralization from altered and/or barren rocks, as indicated by the PC_E1 and PC_M1 components developed during this study. However, these two classification approaches provide different information on the nature of mineralization and alteration present in a given area, as indicated by second and third principal components. The PC_E2 component allows the discrimination of hydrothermally altered rocks from unaltered rocks, whereas PC_M2 distinguishes between different types of mineralization (e.g., disseminated vs. vein-hosted). Element and mineral mineralization indexes (EMI and MMI) extracted from PC_E1 and PC_M1 are consistent with textural observations on a hand specimen scale, and can be used in gold mineralization exploration in under-explored regions.

Declaration of Competing Interest

The authors declare that they have no known competing financial interests or personal relationships that could have appeared to influence the work reported in this paper.

Acknowledgements

We thank Lucille Daver for size-fraction sample preparation that contributed significantly to this work. We also thank Michel Preda for the XRF and XRD analyses undertaken during this study. Finally, this work could not have been completed without the support of FQRNT, Géologie Québec, the contribution of industrial partners to the Corridor Project, and funds from the China Scholarship Council (CSC no. 201604910464), the Department of Science and Technology of Guizhou Province (Guizhou Science Foundation 20171197), and the "CAS Hundred Talents Program" (project Y9CJ034000). We thank Pierre Bedeaux and Kristoffer Szilas for constructive reviews, and Franco Pirajno and M. Santosh for editorial handling.

Appendix A. Supplementary data

Supplementary data to this article can be found online at https://doi.org/10.1016/j.oregeorev.2020.103840.

References

Aitchison, J., 1986. The statistical analysis of compositional data. Chapman and Hall Ltd., London (UK), pp. 365–374.
Bajwah, Z.U., Seccombe, P.K., Offler, R., 1987. Trace element distribution Co: Ni ratios and genesis of the Big Cadia iron-copper deposit, New South Wales, Australia. Miner. Deposita 22, 292–300.
Beaudoin, G., Chiaradia, M., 2016. Fluid mixing in orogenic gold deposits: evidence from the H-O-Sr isotope composition of the Val-d'Or vein field (Abitibi, Canada). Chem. Geol. 437, 7–18.
Beaudoin, G., Pitre, D., 2005. Stable isotope geochemistry of the Archean Val-d'Or (Canada) orogenic gold vein field. Miner. Deposita 40, 59–75.
Bedeaux, P., Pilote, P., Daigneault, R., Rafini, S., 2017. Synthesis of the structural evolution and associated gold mineralization of the Cadillac Fault, Abitibi, Canada. Ore Geol. Rev. 82, 49–69.
Bedeaux, P., Rafini, S., Pilote, P., Daigneault, R., 2018. Modelling Seismically Induced Mesothermal Goldfields along the Deep-Rooted Cadillac-Larder Lake Fault, Abitibi, Canada. Geofluids 2018, Article ID 9479528, 21 pages.
Belkabir, A., Robert, F., Vu, L., Hubert, C., 1993. The influence of dikes on auriferous shear zone development within granitoid intrusions: the Bourlamaque pluton, Val-d'Or district, Abitibi greenstone belt. Can. J. Earth Sci. 30, 1924–1933.
Chandrajith, R., Dissanayake, C.B., Tobschall, H.J., 2001. Application of multi-element relationships in stream sediments to mineral exploration: a case study of Walawe Ganga Basin, Sri Lanka. Appl. Geochem. 16, 339–350.
Chen, S., Hattori, K., Grunsky, E.C., 2018. Multielement statistical evidence for uraniferous hydrothermal activity in sandstones overlying the Phoenix uranium deposit, Athabasca Basin, Canada. Miner. Deposita 53, 493–508.
Cheng, Q., Bonham-Carter, G., Wang, W., Zhang, S., Li, W., Xia, Q., 2011. A spatially weighted principal component analysis for multi-element geochemical data for mapping locations of felsic intrusions in the Gejiu mineral district of Yunnan, China. Comput. Geosci. 37, 662–669.
Clauer, N., Chaudhuri, S., 1998. Isotopic dating of very low-grade metasedimentary and metavolcanic rocks: techniques and methods. In: Frey, M., Robinson, D. (Eds.), Low-grade Metamorphism. Blackwell Publishing Ltd., Oxford, UK, pp. 202–226.
Colvine, A., 1989. An empirical model for the formation of Archean gold deposits: products of final cratonization of the Superior Province, Canada. Econ. Geol. Mono. 6, 37–53.
Colvine, A.C., Andrews, A.J., Cherry, M.E., Durocher, M.E., Fyon, J.A., Lavigne, M.J., Macdonald, A.J., Marmont, S., Poulsen, K.H., Springer, J.S., Troop, D.G., 1984. An integrated model for the origin of Archean lode-gold deposits. Ontario Ministry Nat. Resour. 98.
Cook, H., Johnson, P., Matti, J., Zemmels, I., 1975. IV. Methods of sample preparation, and X-ray diffraction data analysis, X-ray mineralogy laboratory, Deep Sea Drilling Project, University of California, Riverside. Init. Repts. Deep Sea Drill. Proj. 25, 999–1007.
Corfu, F., 1993. The evolution of the southern Abitibi greenstone belt in light of precise U-Pb geochronology. Econ. Geol. 88, 1323–1340.
Couture, J.-F., Pilote, P., Machado, N., Desrochers, J.-P., 1994. Timing of gold mineralization in the Val-d'Or District, southern Abitibi Belt; evidence for two distinct mineralizing events. Econ. Geol. 89, 1542–1551.
Couture, J.F., Pilote, P., 1993. The geology and alteration patterns of a disseminated, shear zone-hosted mesothermal gold deposit; the Francoeur 3 Deposit, Rouyn-Noranda, Quebec. Econ. Geol. 88, 1664–1684.
Cowan, E.J., 2020. Deposit-scale structural architecture of the Sigma-Lamaque gold deposit, Canada—insights from a newly proposed 3D method for assessing structural controls from drill hole data. Miner. Deposita 55, 217–240.
Crosta, A., De Souza Filho, C., Azevedo, F., Brodie, C., 2003. Targeting key alteration minerals in epithermal deposits in Patagonia, Argentina, using ASTER imagery and principal component analysis. Int. J. Remote Sens. 24, 4233–4240.
Daigneault, R., Mueller, W., Chown, E., 2002. Oblique Archean subduction: accretion and exhumation of an oceanic arc during dextral transpression, Southern Volcanic Zone, Abitibi Subprovince Canada. Precamb. Res. 115, 261–290.
Daigneault, R., Mueller, W.U., Chown, E.H., 2004. Abitibi greenstone belt plate tectonics: the diachronous history of arc development, accretion and collision. Dev. Precamb. Geol. 12, 88–103.
Daver, L., 2017. Apport de l'analyse des tourmalines et des pyrite à LA genése des gisements orogéniques Archéens du district de Val-d'Or, Abitibi, Canada [Master]. Université du Québec à Montréal (UQAM).
Daver, L., Sasseville, C., Jébrak, M., 2015. Tourmaline-Pyrite Assemblage in Gold Mineralization of Cadillac Fault in Abitibi, Quebec. Mineral resources in a sustainable world.In: Proceedings of 13th Biennial SGA Meeting, Nancy, Franc , pp. 711–712.
Daver, L., Jébrak, M., Beaudoin, G., Trumbull, R.B., 2020. Three-stage formation of greenstone-hosted orogenic gold deposits in the val-d'or mining district, abitibi, canada: evidence from pyrite and tourmaline. Ore Geol. Rev. 120, 103449.
Davis, J.C., 1986. Statistics and Data Analysis in Geology, third ed. John Wiley and Sons Inc, New York.
De Souza, S., Dubé, B., McNicoll, V., Dupuis, C., Mercier-Langevin, P., Creaser, R.A., Kjarsgaard, I., Monecke, T., Mercier-Langevin, P., Dubé, B., 2017. Geology and Hydrothermal Alteration of the World-Class Canadian Malartic Gold Deposit: Genesis of an Archean Stockwork-Disseminated Gold Deposit in the Abitibi Greenstone Belt. In: Monecke, T., Mercier-Langevin, P., Dubé, B. (Eds.), Archean Base and Precious Metal Deposits, Southern Abitibi Greenstone Belt, Canada. Society of Economic Geologists, Littleton, USA, pp. 263–291.
Dubé, B., Gosselin, P., Mercier-Langevin, P., Hannington, M., Galley, A., 2007. Gold-rich volcanogenic massive sulphide deposits. In: Goodfellow, W. (Ed.), Mineral Deposits of Canada - A Synthesis of Major Deposit Types, District Metallogeny, The Evolution of Geological Provinces and Exploration Methods. Geological Association of Canada, Mineral Deposits Division Special Publication, vol. 5, pp. 75–94.
Dubé, B., Mercier-Langevin, P., Ayer, J., Atkinson, B., Monecke, T., Monecke, T., Mercier-Langevin, P., Dubé, B., 2017. Orogenic greenstone-hosted quartz-carbonate gold deposits of the Timmins-porcupine camp. In: Monecke, T., Mercier-Langevin, P.,

Dubé, B. (Eds.), Archean Base and Precious Metal Deposits, Southern Abitibi Greenstone Belt, Canada. Society of Economic Geologists, Littleton, USA, pp. 51–79.
Eilu, P., Mikucki, E.J., 1998. Alteration and primary geochemical dispersion associated with the Bulletin lode-gold deposit, Wiluna, Western Australia. J. Geochem. Explor. 63, 73–103.
Faure, S., 2009. Reconnaissance des failles synvolcaniques fertiles pour les SMV dans les ceintures de roches vertes déformées: application dans le secteur de Val-d'Or, p. 46.
Fayol, N., Jébrak, M., Harris, L.B., 2016. The magnetic signature of Neoarchean alkaline intrusions and their related gold deposits: Significance and exploration implications. Precamb. Res. 283, 13–23.
Gaillard, N., Williams-Jones, A.E., Clark, J.R., Lypaczewski, P., Salvi, S., Perrouty, S., Piette-Lauzière, N., Guilmette, C., Linnen, R.L., 2018. Mica composition as a vector to gold mineralization: deciphering hydrothermal and metamorphic effects in the Malartic District, Québec. Ore Geol. Rev. 95, 789–820.
Goldfarb, R., Groves, D., Gardoll, S., 2001. Orogenic gold and geologic time: a global synthesis. Ore Geol. Rev. 18, 1–75.
Goldfarb, R.J., Baker, T., Dube, B., Groves, D.I., Hart, C.J.R., Gosselin, P., 2005. Distribution, character, and genesis of gold deposits in metamorphic terranes. In: Economic Geology 100th Anniversary Volume, pp. 407–450.
Goodwin, A., 1982. Archean volcanoes in southwestern Abitibi belt, Ontario and Quebec: form, composition, and development. Can. J. Earth Sci. 19, 1140–1155.
Groves, D.I., Goldfarb, R.J., Gebre-Mariam, M., Hagemann, S., Robert, F., 1998. Orogenic gold deposits: a proposed classification in the context of their crustal distribution and relationship to other gold deposit types. Ore Geol. Rev. 13, 7–27.
Groves, D.I., Santosh, M., Goldfarb, R.J., Zhang, L., 2018. Structural geometry of orogenic gold deposits: Implications for exploration of world-class and giant deposits. Geosci. Front. 9, 1163–1177.
Grunsky, E.C., 2010. The interpretation of geochemical survey data. Geochem. Explor. Environ. Anal. 10, 27–74.
Hudyma, M., Frenette, P., Leslie, I., 2010. Monitoring open stope caving at Goldex Mine. Min. Technol. 119, 142–150.
Jébrak, M., LeQuentrec, M.F., Mareschal, J.-C., Blais, D., 1991. A gravity survey across the Bourlamaque massif, southeastern Abitibi greenstone belt, Québec, Canada: the relationship between the geometry of tonalite plutons and associated gold mineralization. Precamb. Res. 50, 261–268.
Jolly, W.T., 1978. Metamorphic history of the Archean Abitibi belt. In: Fraser, I.A., Heyward, W.W. (Eds.), Metamorphism in the Canadian Shield. Geological Survey of Canada, Paper, vol. 16, pp. 63–78.
Kerrich, R., King, R., 1993. Hydrothermal zircon and baddeleyite in Val-d'Or Archean mesothermal gold deposits: characteristics, compositions, and fluid-inclusion properties, with implications fortiming of primary gold mineralization. Can. J. Earth Sci. 30, 2334–2351.
Kreuzer, O.P., Buckingham, A., Mortimer, J., Walker, G., Wilde, A., Appiah, K., 2019. An integrated approach to the search for gold in a mature, data-rich brownfields environment: a case study from Sigma-Lamaque, Quebec. Ore Geol. Rev. 111, 102977.
Lemarchand, J., 2012. Les minéralisations filoniennes aurifères du pluton de Bourlamaque (Val d'Or, Abitibi): synthèse structurale et apports de la datation 40Ar/39Ar [Ph.D]. Université du Québec à Montréal (UQAM) and Rennes University.
Longerich, H.P., 1995. Analysis of pressed pellets of geological samples using wavelength-dispersive x-ray fluorescence spectrometry. X-Ray Spectrometry 24, 123–136.
Makvandi, S., Ghasemzadeh-Barvarz, M., Beaudoin, G., Grunsky, E.C., McClenaghan, M. B., Duchesne, C., 2016. Principal component analysis of magnetite composition from volcanogenic massive sulfide deposits: Case studies from the Izok Lake (Nunavut, Canada) and Halfmile Lake (New Brunswick, Canada) deposits. Ore Geol. Rev. 72, 60–85.
McCuaig, T.C., Kerrich, R., 1998. P—T—t—deformation—fluid characteristics of lode gold deposits: evidence from alteration systematics. Ore Geol. Rev. 12, 381–453.
McNicoll, V., Goutier, J., Dubé, B., Mercier-Langevin, P., Ross, P.-S., Dion, C., Monecke, T., Legault, M., Percival, J., Gibson, H., 2014. U-Pb geochronology of the blake river group, abitibi greenstone belt, quebec, and implications for base metal exploration. Econ. Geol. 109, 27–59.
Meng, Y.-M., Sasseville, C., Jébrak, M., 2017. Geochemical assemblages in orogenic gold deposits of the Abitibi greenstore belt, Canada: Constrains from PCA analysis. Mineral resources to discover. In: 14th Biennial SGA Meeting 20-23 August 2017, Proceedings, vol. 2, Quebec City, Canada: Society for Geology Applied to Mineral Deposits (SGA), pp. 171–174.
Meng, Y.-M., Hu, R.-Z., Huang, X.-W., Gao, J.-F., Sasseville, C., 2019. The origin of Huize carbonate-hosted Zn–Pb–Ag deposit in Yunnan province, SW China: constraints from trace element and sulfur isotopic compositions of pyrite. Mineral. Petrol. 113, 369–391.
Mercier-Langevin, P., Simard, M., Dubuc, R., Côté, J., Doucet, P., Daigneault, R., Gaboury, D., Monecke, T., Mercier-Langevin, P., Dubé, B., 2017. Geology of the Lapa Orogenic Gold Deposit. In: Monecke, T., Mercier-Langevin, P., Dubé, B. (Eds.), Archean Base and Precious Metal Deposits, Southern Abitibi Greenstone Belt, Canada. Society of Economic Geologists, Littleton, USA, pp. 247–262.
Mériaud, N., Jébrak, M., 2017. From intrusion-related to orogenic mineralization: the Wasamac Deposit, Abitibi greenstone belt. Canada. Ore Geol. Rev. 84, 289–308.
Monecke, T., Mercier-Langevin, P., Dubé, B., Frieman, B.M., Monecke, T., Mercier-Langevin, P., Dubé, B., 2017. Geology of the Abitibi Greenstone Belt. In: Monecke, T., Mercier-Langevin, P., Dubé, B. (Eds.), Archean Base and Precious Metal Deposits, Southern Abitibi Greenstone Belt, Canada. Society of Economic Geologists, Littleton, USA, pp. 7–49.
Naldrett, A.J., 2004. Magmatic sulfide deposits: Geology, geochemistry and exploration. Springer, New York, pp. 1–730.
Neumayr, P., Hagemann, S., Couture, J.-F., 2000. Structural setting, textures, and timing of hydrothermal vein systems in the Val d'Or camp, Abitibi, Canada: implications for the evolution of transcrustal, second-and third-order fault zones and gold mineralization. Can. J. Earth Sci. 37, 95–114.
Neumayr, P., Hagemann, S.G., Banks, D.A., Yardley, B.W.D., Couture, J.-F., Landis, G.P., Rye, R., 2007. Fluid chemistry and evolution of hydrothermal fluids in an Archaean transcrustal fault zone network: the case of the Cadillac Tectonic Zone, Abitibi greenstone belt, Canada. Can. J. Earth Sci. 44, 745–773.
Norusis, M., 2008. SPSS 16.0 statistical procedures companion. Prentice Hall Press.
Poirier, S., Roy, L., D'Amours, C., Gaudreault, D., Utiger, M., Ilieva, T., Bergeron, S., 2005. 43–101 Technical report and fall 2015 mineral resource estimate update for the Lamaque project. Integra Gold Corp 1–403.
Poulsen, K.H., Monecke, T., Mercier-Langevin, P., Dubé, B., 2017. The Larder Lake-Cadillac Break and Its Gold Districts. In: Monecke, T., Mercier-Langevin, P., Dubé, B. (Eds.), Archean Base and Precious Metal Deposits, Southern Abitibi Greenstone Belt, Canada. Society of Economic Geologists, Littleton, USA, pp. 133–167.
Powell, W., Carmichael, D., Hodgson, C., 1995. Conditions and timing of metamorphism in the southern Abitibi greenstone belt, Quebec. Can. J. Earth Sci. 32, 787–805.
Rabeau, O., Royer, J.-J., Jébrak, M., Cheilletz, A., 2013. Log-uniform distribution of gold deposits along major Archean fault zones. Miner. Deposita 48, 817–824.
Rafini, S., 2014. Typologie des minéralisations aurifères associées à la Faille de Cadillac. Rapport du projet CONSOREM 2011-01 et 2012-01, .p. 45.
Rezeau, H., Moritz, R., Beaudoin, G., 2017. Formation of Archean batholith-hosted gold veins at the Lac Herbin deposit, Val-d'Or district, Canada: Mineralogical and fluid inclusion constraints. Miner. Deposita 52, 421–442.
Robert, F., 1990. Structural setting and control of gold-quartz veins of the Val d'Or area, southeastern Abitibi subprovince. Gold and Base-Metal Mineralization in the Abitibi Subprovince, Canada, with Emphasis on the Quebec Segment. University of Western Australia Short Course Notes 24, 167–210.
Robert, F., 1994. Vein fields in gold districts: The example of Val d'Or, southeastern Abitibi subprovince. Quebec: Geological Survey of Canada. Curr. Res. Paper 1994C, 295–302.
Robert, F., 2001. Syenite-associated disseminated gold deposits in the Abitibi greenstone belt, Canada. Miner. Deposita 36, 503–516.
Robert, F., Boullier, A.M., Firdaous, K., 1995. Gold-quartz veins in metamorphic terranes and their bearing on the role of fluids in faulting. J. Geophys. Res. Solid Earth 100, 12861–12879.
Robert, F., Poulsen, K., 1997. World-class Archaean gold deposits in Canada: an overview. Aust. J. Earth Sci. 44, 329–351.
Robert, F., Poulsen, K.H., 2001. Vein formation and deformation in greenstone gold deposits. Rev. Econ. Geol. 14, 111–155.
Robert, F., Poulsen, K.H., Cassidy, K.F., Hodgson, C.J., 2005. Gold metallogeny of the Superior and Yilgarn cratons. In: Economic Geology 100th Anniversary Volume, pp. 1001–1034.
Sasseville, C., Michel, J., Stevenson, R., André, P., 2015. When size does matter...in gold exploration. Mineral resources in a sustainable world. 13th Biennial SGA Meeting, 24–27 August 2015, Proceedings, vol. 2, Nancy, France: Society for Geology Applied to Mineral Deposits (SGA), pp. 623–626.
Sasseville, C., Jébrak, M., 2017. Gold epichrons in the Abitibi greenstone belt, Canada, and the impact of early Proterozoic Mattachewan LIP event. Mineral resources to discover, 2. Society for Geology Applied to Mineral Deposits (SGA, Quebec City, Canada, pp. 183–186.
Scott, C.R., Mueller, W.U., Pilote, P., 2002. Physical volcanology, stratigraphy, and lithogeochemistry of an Archean volcanic arc: evolution from plume-related volcanism to arc rifting of SE Abitibi Greenstone Belt, Val d'Or, Canada. Precamb. Res. 115, 223–260.
Sibson, R.H., 2004. Controls on maximum fluid overpressure defining conditions for mesozonal mineralisation. J. Struct. Geol. 26, 1127–1136.
Simard, M., Gaboury, D., Daigneault, R., Mercier-Langevin, P., 2013. Multistage gold mineralization at the Lapa mine, Abitibi Subprovince: insights into auriferous hydrothermal and metasomatic processes in the Cadillac-Larder Lake Fault Zone. Miner. Deposita 48, 883–905.
Simon, Q., Hillaire-Marcel, C., St-Onge, G., Andrews, J.T., 2014. North-eastern Laurentide, western Greenland and southern Innuitian ice stream dynamics during the last glacial cycle. J. Quat. Sci. 29, 14–26.
Takahashi, G., 2015. Sample preparation for X-ray fluorescence analysis. Rigaku J. 31, 26–30.
Tessier, A., Trudel, P., Imreh, L., 1990. Petrology and alteration of the Siscoe stock at the Siscoe gold mine, Val d'Or, Quebec. In: Rivé, M., Verpaelst, P., Gagnon, Y., Lullin, J. M., Riverin, G., Simard, A. (Eds.), The northwestern Quebec polymetallic belt. Canadian Institute of Mining and Metallurgy, Special vol. 43, pp. 285–298.
Tremblay, A., 2001. Postmineralization faults in the Beaufor gold deposit, Abitibi greenstone belt, Canada: geometry, origin, and tectonic implications for the Val-d'Or mining district. Econ. Geol. 96, 509–524.
Trépanier, S., Mathieu, L., Daigneault, R., 2015. CONSONORM_LG: new normative minerals and alteration indexes for low-grade metamorphic rocks. Econ. Geol. 110, 2127–2138.
Wilkinson, L., Cruden, A.R., Krogh, T.E., 1999. Timing and kinematics of post-Timiskaming deformation within the Larder Lake-Cadillac deformation zone, southwest Abitibi greenstone belt, Ontario, Canada. Can. J. Earth Sci. 36, 627–647.
Wong, L., Davis, D., Krogh, T., Robert, F., 1991. U-Pb zircon and rutile chronology of Archean greenstone formation and gold mineralization in the Val d'Or region, Quebec. Earth Planet. Sci. Lett. 104, 325–336.